

Behavior of nearby synchronous rotation of a Poincaré-Hough satellite at low eccentricity

Benoît Noyelles

Received: date / Accepted: date

Abstract This paper presents a study of the Poincaré-Hough model of rotation of the synchronous natural satellites, in which these bodies are assumed to be composed of a rigid mantle and a triaxial cavity filled with inviscid fluid of constant uniform density and vorticity. In considering an Io-like body on a low eccentricity orbit, we describe the different possible behaviors of the system, depending on the size, polar flattening and shape of the core.

We use for that the numerical tool. We propagate numerically the Hamilton equations of the systems, before expressing the resulting variables under a quasi-periodic representation. This expression is obtained numerically by frequency analysis. This allows us to characterize the equilibria of the system, and to distinguish the causes of their time variations.

We show that, even without orbital eccentricity, the system can have complex behaviors, in particular when the core is highly flattened. In such a case, the polar motion is forced by several degrees and longitudinal librations appear. This is due to splitting of the equilibrium position of the polar motion. We also get a shift of the obliquity when the polar flattening of the core is small.

Keywords Natural satellites · Rotation · Periodic Orbits · Hamiltonian Systems · Numerical Methods

1 Introduction

Space missions like Galileo for the Jovian system or Cassini for the Saturnian one give us information on the internal structure of the natural satellites, through their gravity fields (Anderson 2001 [1]), observations of their surfaces (Porco et al. 2006 [39]) or measurements of their rotational states (Tiscareno et al. 2009 [46], Lorenz et

FUNDP - The University of Namur
NAmur Center for Complex SYStems (NAXYS)
Belgium
· IMCCE (Paris Observatory / USTL / UPMC)
France
E-mail: benoit.noyelles@fundp.ac.be

al. 2008 [28]). It is known that the internal structure of a body influences its rotational dynamics, especially when this body is locked in a spin-orbit resonance, like the 1:1 resonance for most of the natural satellites of the Solar system, and the 3:2 resonance for Mercury.

There are at least two ways to approach the modelisation of the interactions between the internal structure and the rotational dynamics. One way is to complexify the internal structure, taking account for instance of an atmosphere, a deformable crust, a subsurface ocean, an iron core. . . in a simplified dynamical model that allows to consider only one degree of freedom (see e.g. Rambaux et al. (2011) [41] for the longitudinal libration of satellites having an internal ocean, or Tokano et al. (2011) [47] for the forcing of the polar motion of Titan due to its atmosphere). Another possibility is to consider a simple internal structure model (i.e. to assume the body to be rigid), in a full dynamical model considering several degrees of freedom (longitudinal motion, obliquity, and polar motion) like in (Henrard 2005 [19,20]).

An evolution of this approach is to consider a two-layer body composed of a rigid mantle and an ellipsoidal fluid core in which the flow is laminar and core-mantle interactions result in pressure coupling at the core-mantle boundary. This has been originally written by Hough (1895) [22] and Poincaré (1910) [38] (that is the reason why this model is sometimes called the Poincaré-Hough model), put in Hamiltonian form by Getino & Ferrándiz (see e.g. [13,15]) under general assumptions, and by Touma & Wisdom (2001) [48], and recently used for Io (Henrard 2008 [21]), Mercury (Noyelles et al. 2010 [35]) and the Moon (Meyer & Wisdom 2011 [30]). Another model exists, taking account of the elasticity of the mantle (Getino & Ferrándiz 1995 [14]). This case will not be considered here.

In the case of the 1:1 spin-orbit resonance, the existing studies do not consider a wide range of internal structure parameter. This paper aims at contributing to fill the gap to understand the behavior of the system for any size and shape (provided it is triaxial) of the core. The plan of the study is the following: after a description of the model, we present a systematic numerical study of the system with different sizes and shapes of the core, the considered body being an Io-like body on a low eccentricity orbit with a uniform nodal regression and constant inclination. Then, “unusual” behaviors are highlighted with analytical explanations.

2 The model

In the study of Henrard [21], the size of the core was not constrained, but its shape was assumed to be proportional to the whole Io. We here generalize this approach, in letting the shape parameters vary.

2.1 Physical model

Four references frames are considered (see Fig.1 & 2). The first one, $(\mathbf{e}_1, \mathbf{e}_2, \mathbf{e}_3)$ is assumed to be inertial for the rotational dynamics, it is in fact centered on the satellite and in translation with the inertial reference frame in which the motion of the satellite is defined. The second one, $(\mathbf{n}_1^c, \mathbf{n}_2^c, \mathbf{n}_3^c)$ is linked to the angular momentum of a *pseudo-core* that we define later, while the third one, i.e. $(\mathbf{n}_1, \mathbf{n}_2, \mathbf{n}_3)$, is linked to the total angular momentum of the satellite. Finally, the last one, written as $(\mathbf{f}_1, \mathbf{f}_2, \mathbf{f}_3)$, is rigidly

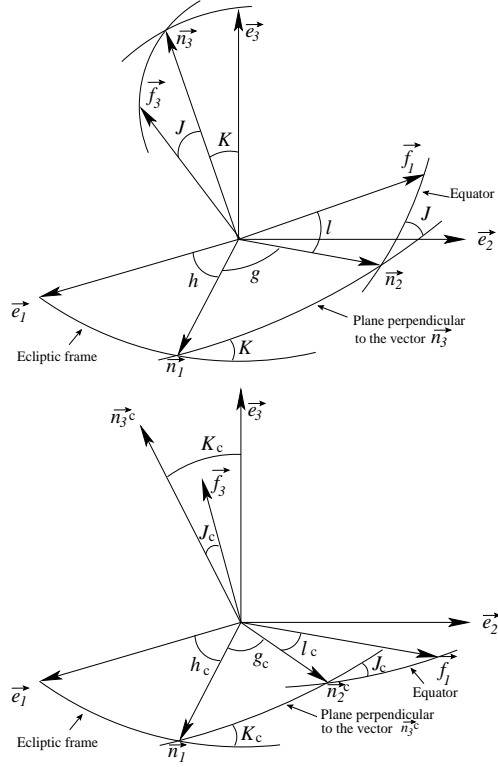


Fig. 1 In the upper panel we have 3 reference frames: one linked to the ecliptic plane ($\mathbf{e}_1, \mathbf{e}_2, \mathbf{e}_3$), another linked to the angular momentum \mathbf{N} ($\mathbf{n}_1, \mathbf{n}_2, \mathbf{n}_3$), and the last one linked to the axes of inertia ($\mathbf{f}_1, \mathbf{f}_2, \mathbf{f}_3$) of the satellite. In the lower panel we have a similar configuration but instead of the angular momentum of the satellite, we have a reference frame linked to the angular momentum of a pseudo-core (defined later). We have the Euler angles (h, K, g) positioning the vector \mathbf{n}_2 on the plane perpendicular to the angular momentum of the satellite and the Euler angles (h_c, K_c, g_c) positioning the vector \mathbf{n}_2^c on the plane perpendicular to the angular momentum of the pseudo-core. The angles (l, J) and (l_c, J_c) position the axis of least inertia. Note that J_c is defined on the other side than J .

linked to the principal axes of inertia of the satellite. In this last reference frame, the matrix of inertia of the satellite reads:

$$I = \begin{pmatrix} A & 0 & 0 \\ 0 & B & 0 \\ 0 & 0 & C \end{pmatrix} \quad (1)$$

with $0 < A \leq B \leq C$, while that of the core is:

$$I_c = \begin{pmatrix} A_c & 0 & 0 \\ 0 & B_c & 0 \\ 0 & 0 & C_c \end{pmatrix}, \quad (2)$$

in the same reference frame. So, the orientations of the mantle and the cavity are the same, a misalignment of their principal axes would require to consider the mantle as elastic, this is beyond the scope of the paper. This would in fact require additional

parameters related to the elasticity of the mantle, see e.g. (Getino & Ferrándiz 1995 [14]).

As for the whole satellite, we have $0 < A_c \leq B_c \leq C_c$. In this way, the principal moments of inertia of the mantle are respectively $A_m = A - A_c$, $B_m = B - B_c$ and $C_m = C - C_c$. The principal elliptical radii of the cavity are written respectively a , b , c , yielding

$$\begin{aligned} A_c &= \iiint (x_2^2 + x_3^2) \rho \, dx_1 \, dx_2 \, dx_3 = \frac{M_c}{5} (b^2 + c^2), \\ B_c &= \iiint (x_1^2 + x_3^2) \rho \, dx_1 \, dx_2 \, dx_3 = \frac{M_c}{5} (a^2 + c^2), \\ C_c &= \iiint (x_1^2 + x_2^2) \rho \, dx_1 \, dx_2 \, dx_3 = \frac{M_c}{5} (a^2 + b^2), \end{aligned}$$

where ρ and M_c are respectively the mass density and the mass of the fluid core, the quadrature being performed over the volume of the core.

2.2 The kinetic energy of the system

A Hamiltonian formulation of such a problem is usually composed of a kinetic energy and a disturbing potential, here the perturbation of the planet. Therefore, we consider every internal process, as the core-mantle interactions in our case, as part of the kinetic energy of the satellite. This section is widely inspired from (Henrard 2008 [21]).

The components (v_1, v_2, v_3) of the velocity field at the location (x_1, x_2, x_3) inside the liquid core, in the frame of the principal axes of inertia of the mantle, are assumed to be (Poincaré 1910 [38]):

$$v_1 = \left(\omega_2 + \frac{a}{c} \nu_2 \right) x_3 - \left(\omega_3 + \frac{a}{b} \nu_3 \right) x_2, \quad (3)$$

$$v_2 = \left(\omega_3 + \frac{b}{a} \nu_3 \right) x_1 - \left(\omega_1 + \frac{b}{c} \nu_1 \right) x_3, \quad (4)$$

$$v_3 = \left(\omega_1 + \frac{c}{b} \nu_1 \right) x_2 - \left(\omega_2 + \frac{c}{a} \nu_2 \right) x_1, \quad (5)$$

where $(\omega_1, \omega_2, \omega_3)$ are the components of the angular velocity of the mantle with respect to an inertial frame, and the vector of coordinates (ν_1, ν_2, ν_3) specifies the velocity field of the core with respect to the moving mantle. This vector is the velocity of a given fluid particle. Here we assume that this velocity field (ν_1, ν_2, ν_3) depends only on the time t , and not on the spatial coordinates (x_1, x_2, x_3) . It implies that we have

$$\nabla \cdot \mathbf{v} = \frac{\partial v}{\partial x_1} + \frac{\partial v}{\partial x_2} + \frac{\partial v}{\partial x_3} = 0, \quad (6)$$

this equation is known as the continuity equation.

The angular momentum of the core \mathbf{N}'_c is obtained by:

$$\mathbf{N}'_c = \iiint_{core} (\mathbf{x} \times \mathbf{v}) \rho \, dx_1 \, dx_2 \, dx_3 \quad (7)$$

and the result is:

$$\begin{aligned}
\mathbf{N}'_c &= \frac{M_c}{5} \left[\left(\frac{c}{b} \nu_1 + \omega_1 \right) b^2 + \left(\frac{b}{c} \nu_1 + \omega_1 \right) c^2 \right] \mathbf{f}_1 \\
&+ \frac{M_c}{5} \left[\left(\frac{c}{a} \nu_2 + \omega_2 \right) a^2 + \left(\frac{a}{c} \nu_2 + \omega_2 \right) c^2 \right] \mathbf{f}_2 \\
&+ \frac{M_c}{5} \left[\left(\frac{b}{a} \nu_3 + \omega_3 \right) a^2 + \left(\frac{a}{b} \nu_3 + \omega_3 \right) b^2 \right] \mathbf{f}_3.
\end{aligned} \tag{8}$$

We now set the following quantities:

$$\begin{aligned}
D_1 &= \frac{2M_c}{5} bc = \sqrt{(A_c - B_c + C_c)(A_c + B_c - C_c)}, \\
D_2 &= \frac{2M_c}{5} ac = \sqrt{(-A_c + B_c + C_c)(A_c + B_c - C_c)}, \\
D_3 &= \frac{2M_c}{5} ab = \sqrt{(-A_c + B_c + C_c)(A_c - B_c + C_c)},
\end{aligned}$$

that have the dimension of moments of inertia and can be seen as parameters of the core as A_c , B_c and C_c , and we can write:

$$\mathbf{N}'_c = [A_c \omega_1 + D_1 \nu_1] \mathbf{f}_1 + [B_c \omega_2 + D_2 \nu_2] \mathbf{f}_2 + [C_c \omega_3 + D_3 \nu_3] \mathbf{f}_3, \tag{9}$$

while the angular momentum of the mantle is

$$\mathbf{N}_m = A_m \omega_1 \mathbf{f}_1 + B_m \omega_2 \mathbf{f}_2 + C_m \omega_3 \mathbf{f}_3, \tag{10}$$

and the total angular momentum of the satellite is

$$\mathbf{N} = [A \omega_1 + D_1 \nu_1] \mathbf{f}_1 + [B \omega_2 + D_2 \nu_2] \mathbf{f}_2 + [C \omega_3 + D_3 \nu_3] \mathbf{f}_3. \tag{11}$$

The kinetic energy of the core is

$$T_c = \frac{1}{2} \iiint_{core} \rho v^2 dx_1 dx_2 dx_3 \tag{12}$$

i.e.¹

$$T_c = \frac{1}{2} (A_c(\omega_1^2 + \nu_1^2) + B_c(\omega_2^2 + \nu_2^2) + C_c(\omega_3^2 + \nu_3^2) + 2D_1 \omega_1 \nu_1 + 2D_2 \omega_2 \nu_2 + 2D_3 \omega_3 \nu_3), \tag{13}$$

while the kinetic energy of the mantle T_m is

$$T_m = \frac{1}{2} \mathbf{N}_m \cdot \boldsymbol{\omega} = \frac{A_m \omega_1^2 + B_m \omega_2^2 + C_m \omega_3^2}{2}. \tag{14}$$

From $T = T_m + T_c$ we finally deduce the kinetic energy of the satellite:

$$T = \frac{1}{2} (A \omega_1^2 + B \omega_2^2 + C \omega_3^2 + A_c \nu_1^2 + B_c \nu_2^2 + C_c \nu_3^2 + 2D_1 \omega_1 \nu_1 + 2D_2 \omega_2 \nu_2 + 2D_3 \omega_3 \nu_3). \tag{15}$$

We can easily check the expressions of the partial derivatives, for instance

¹ we here correct a misprint present in Eq.13 of (Noyelles et al. 2010 [35])

$$\frac{\partial T}{\partial \omega_1} = A\omega_1 + D_1\nu_1 = N_1 \quad (16)$$

or

$$\frac{\partial T}{\partial \nu_1} = D_1\omega_1 + A_c\nu_1 = N_1^c, \quad (17)$$

where N_i are the components of the total angular momentum. N_i^c are not the components of the angular momentum of the core but are close to it for a cavity close to spherical. We have, for instance for the first component:

$$N_1^c - N_1'^c = (A_c - D_1)(\omega_1 - \nu_1) = \frac{M_c}{5}(c - b)^2(\omega_1 - \nu_1), \quad (18)$$

so the difference is of the second order in departure from the sphericity. From now on, we call *angular momentum of the pseudo-core* the vector $\mathbf{N}^c = N_1^c \mathbf{f}_1 + N_2^c \mathbf{f}_2 + N_3^c \mathbf{f}_3$.

With these notations, the Poincaré-Hough's equations of motion, for the system mantle-core in the absence of external torque, are (see e.g. Eq.15 in [48] or [21]):

$$\frac{d\mathbf{N}}{dt} = \mathbf{N} \times \nabla_{\mathbf{N}} \mathcal{T}, \quad (19)$$

$$\frac{d\mathbf{N}^c}{dt} = \mathbf{N}^c \times \nabla_{-\mathbf{N}^c} \mathcal{T}, \quad (20)$$

with

$$\nabla_{\mathbf{N}} \mathcal{T} = \frac{\partial \mathcal{T}}{\partial N_1} \mathbf{f}_1 + \frac{\partial \mathcal{T}}{\partial N_2} \mathbf{f}_2 + \frac{\partial \mathcal{T}}{\partial N_3} \mathbf{f}_3, \quad (21)$$

and

$$\nabla_{-\mathbf{N}^c} \mathcal{T} = -\frac{\partial \mathcal{T}}{\partial N_1^c} \mathbf{f}_1 - \frac{\partial \mathcal{T}}{\partial N_2^c} \mathbf{f}_2 - \frac{\partial \mathcal{T}}{\partial N_3^c} \mathbf{f}_3. \quad (22)$$

Here \mathcal{T} is the kinetic energy expressed in terms of the components of the vectors \mathbf{N} and \mathbf{N}^c , i.e.

$$\begin{aligned} \mathcal{T} = & \frac{1}{2\alpha} (A_c N_1^2 + A(N_1^c)^2 - 2D_1 N_1 N_1^c) + \frac{1}{2\beta} (B_c N_2^2 + B(N_2^c)^2 - 2D_2 N_2 N_2^c) \\ & + \frac{1}{2\gamma} (C_c N_3^2 + C(N_3^c)^2 - 2D_3 N_3 N_3^c) \end{aligned} \quad (23)$$

with $\alpha = AA_c - D_1^2$, $\beta = BB_c - D_2^2$ and $\gamma = CC_c - D_3^2$.

2.3 The Hamiltonian

2.3.1 The rotational kinetic energy

We assume that the cavity and the satellite are almost spherical, this allows us to introduce the four small parameters ϵ_i :

$$\epsilon_1 = \frac{2C - A - B}{2C} = J_2 \frac{MR^2}{C}, \quad (24)$$

$$\epsilon_2 = \frac{B - A}{2C} = 2C_{22} \frac{MR^2}{C}, \quad (25)$$

$$\epsilon_3 = \frac{2C_c - A_c - B_c}{2C_c}, \quad (26)$$

$$\epsilon_4 = \frac{B_c - A_c}{2C_c}, \quad (27)$$

where M is the mass of our body and R its mean radius, and also the parameter $\delta = C_c/C$, i.e. the ratio between the polar inertial momentum of the core and of the satellite. ϵ_1 represents the polar flattening of the satellite, while ϵ_2 is its equatorial ellipticity. ϵ_3 and ϵ_4 have the same meaning for the cavity. If we assume the core of the satellite to be spherical, we should take $\epsilon_3 = \epsilon_4 = 0$, while $\epsilon_4 = 0$ represents an axisymmetric cavity. Henrard [21] considered that the ellipsoid of inertia of the core and the mantle were proportional, the mathematical formulation was $\epsilon_3 = \epsilon_1$ and $\epsilon_4 = \epsilon_2$.

We now introduce the two sets of Andoyer's variables [2], (l, g, h, L, G, H) and $(l_c, g_c, h_c, L_c, G_c, H_c)$, related respectively to the whole satellite and to its core. The angles (h, K, g) are the Euler angles of the vector \mathbf{n}_2 , node of the equatorial plane over the plane perpendicular to the angular momentum \mathbf{N} , the angles (J, l) position the axis of least inertia \mathbf{f}_1 with respect to \mathbf{n}_2 . Correspondingly the angles (h_c, K_c, g_c) are the Euler angles of the vector \mathbf{n}_2^c , node of the equatorial plane over the plane perpendicular to the angular momentum of the pseudo-core \mathbf{N}^c , and (J_c, l_c) position the axis of least inertia with respect to \mathbf{n}_2^c . The Figure 2 shows a schematic view of all the reference frames and relevant angles. The variables are (h, g, l) and (h_c, g_c, l_c) and the corresponding momenta ($H = N \cos K$, $G = N$, $L = N \cos J$) and ($H_c = N^c \cos K_c$, $G_c = N^c$, $L_c = N^c \cos J_c$). Expressed in Andoyer's variables the components of \mathbf{N} and \mathbf{N}^c are:

$$\begin{aligned} N_1 &= \sqrt{G^2 - L^2} \sin l, & N_1^c &= \sqrt{G_c^2 - L_c^2} \sin l_c, \\ N_2 &= \sqrt{G^2 - L^2} \cos l, & N_2^c &= \sqrt{G_c^2 - L_c^2} \cos l_c, \\ N_3 &= L, & N_3^c &= L_c. \end{aligned}$$

We can now straightforwardly derive the Hamiltonian \mathcal{H}_1 of the free rotation of the satellite, using Andoyer's variables and changing the sign of \mathbf{N}^c to take the minus sign of the Poincaré-Hough equations into account (Eq.20). We also linearize the Hamiltonian with respect to the small parameters ϵ_i (their orders of magnitude being about 10^{-5} , see Tab.1), and get:

$$\begin{aligned}
p &= l + g + h, & P &= \frac{G}{nC}, \\
r &= -h, & R &= P(1 - \cos K), \\
\xi_1 &= -\sqrt{2P(1 - \cos J)} \sin l, & \eta_1 &= \sqrt{2P(1 - \cos J)} \cos l, \\
p_c &= -l_c + g_c + h_c, & P_c &= \frac{G_c}{nC}, \\
r_c &= -h_c, & R_c &= P_c(1 - \cos K_c), \\
\xi_2 &= \sqrt{2P_c(1 + \cos J_c)} \sin l_c, & \eta_2 &= \sqrt{2P_c(1 + \cos J_c)} \cos l_c.
\end{aligned} \tag{29}$$

The first three lines of this new set of variables and associated moments are related to the whole body, while the last three ones are related to the pseudo-core. P is the normalized norm of the angular momentum, it should be close to 1 at the spin-orbit resonance. Since the obliquity K is small, we have $R \propto K^2$, i.e. this is a small quantity related to the obliquity of the body. The quantities (ξ_1, η_1) are related to the polar motion of the body, i.e. the angle J between the geometrical polar axis and the angular momentum, while l is the precession angle associated. We can note that ξ_1 and η_1 are always defined, while l is not defined when $J = 0$. The last three lines have basically the same meaning for the pseudo-core. We will see later that the degree of freedom (r_c, R_c) is in fact not involved in the dynamics of this model, and that p_c is not involved either, letting the norm of the angular momentum of the pseudo-core P_c to be a constant. So, we can consider that the rotational dynamics of our body has 4, and not 6, degrees of freedom.

In order to be consistent with the minus sign in the equations and before l_c , the amplitude of the wobble of the pseudo-core J_c has to be replaced by $\pi - J_c$. In this way, we have $L_c = G_c \cos(\pi - J_c) = -G_c \cos(J_c)$. In this new set of variables, we have

$$\begin{aligned}
N_1 &= -nC \sqrt{P^2 - \left(P - \frac{\xi_1^2 + \eta_1^2}{2}\right)^2} \frac{\xi_1}{\xi_1^2 + \eta_1^2}, & N_1^c &= nC \sqrt{P_c^2 - \left(\frac{\xi_2^2 + \eta_2^2}{2} - P_c\right)^2} \frac{\xi_2}{\xi_2^2 + \eta_2^2}, \\
N_2 &= nC \sqrt{P^2 - \left(P - \frac{\xi_1^2 + \eta_1^2}{2}\right)^2} \frac{\eta_1}{\xi_1^2 + \eta_1^2}, & N_2^c &= nC \sqrt{P_c^2 - \left(\frac{\xi_2^2 + \eta_2^2}{2} - P_c\right)^2} \frac{\eta_2}{\xi_2^2 + \eta_2^2}, \\
N_3 &= nC \left(P - \frac{\xi_1^2 + \eta_1^2}{2}\right), & N_3^c &= nC \left(\frac{\xi_2^2 + \eta_2^2}{2} - P_c\right),
\end{aligned}$$

and the Hamiltonian of the free rotational motion becomes, after division by nC :

$$\begin{aligned}
\mathcal{H}_1 = & \frac{n}{2(1-\delta)} \left(P^2 + \frac{P_c^2}{\delta} + 2\sqrt{\left(P - \frac{\xi_1^2 + \eta_1^2}{4}\right)\left(P_c - \frac{\xi_2^2 + \eta_2^2}{4}\right)} (\eta_1\eta_2 - \xi_1\xi_2) \right. \\
& \left. + 2\left(P - \frac{\xi_1^2 + \eta_1^2}{2}\right)\left(\frac{\xi_2^2 + \eta_2^2}{2} - P_c\right) \right) \\
& + \frac{n\epsilon_1}{2(1-\delta)^2} \left(P_c^2 - \left(\frac{\xi_2^2 + \eta_2^2}{2} - P_c\right)^2 + P^2 - \left(P - \frac{\xi_1^2 + \eta_1^2}{2}\right)^2 \right. \\
& \left. + 2\sqrt{\left(P - \frac{\xi_1^2 + \eta_1^2}{4}\right)\left(P_c - \frac{\xi_2^2 + \eta_2^2}{4}\right)} (\eta_1\eta_2 - \xi_1\xi_2) \right) \\
& + \frac{n\epsilon_2}{2(1-\delta)^2} \left(\frac{1}{4}(4P - \xi_1^2 - \eta_1^2)(\xi_1^2 - \eta_1^2) + \frac{1}{4}(4P_c - \xi_2^2 - \eta_2^2)(\xi_2^2 - \eta_2^2) \right. \\
& \left. - 2\sqrt{\left(P - \frac{\xi_1^2 + \eta_1^2}{4}\right)\left(P_c - \frac{\xi_2^2 + \eta_2^2}{4}\right)} (\eta_1\eta_2 + \xi_1\xi_2) \right) \\
& - \frac{n\epsilon_3}{2(1-\delta)^2} \left(\delta\left(P^2 - \left(P - \frac{\xi_1^2 + \eta_1^2}{2}\right)^2\right) + \left(P_c^2 - \left(\frac{\xi_2^2 + \eta_2^2}{2} - P_c\right)^2\right)\left(2 - \frac{1}{\delta}\right) \right. \\
& \left. + 2\delta\sqrt{\left(P - \frac{\xi_1^2 + \eta_1^2}{4}\right)\left(P_c - \frac{\xi_2^2 + \eta_2^2}{4}\right)} (\eta_1\eta_2 - \xi_1\xi_2) \right) \\
& + \frac{n\epsilon_4}{2(1-\delta)^2} \left(\frac{\delta}{4}(4P - \xi_1^2 - \eta_1^2)(\eta_1^2 - \xi_1^2) + \left(2 - \frac{1}{\delta}\right)\frac{1}{4}(4P_c - \xi_2^2 - \eta_2^2)(\eta_2^2 - \xi_2^2) \right. \\
& \left. + 2\delta\sqrt{\left(P - \frac{\xi_1^2 + \eta_1^2}{4}\right)\left(P_c - \frac{\xi_2^2 + \eta_2^2}{4}\right)} (\eta_1\eta_2 + \xi_1\xi_2) \right). \tag{30}
\end{aligned}$$

Finally, in order to get an easy-to-read formula, we can develop this Hamiltonian up to the second order in $(\xi_1, \xi_2, \eta_1, \eta_2)$ to get:

$$\begin{aligned}
\mathcal{H}_1 \approx & \frac{n}{2(1-\delta)} \left(P^2 + \frac{P_c^2}{\delta} + 2\sqrt{PP_c}(\eta_1\eta_2 - \xi_1\xi_2) \right. \\
& \left. + 2\left(P\frac{\xi_2^2 + \eta_2^2}{2} + P_c\frac{\xi_1^2 + \eta_1^2}{2} - PP_c \right) \right) \\
& + \frac{n\epsilon_1}{2(1-\delta)^2} \left(P(\xi_1^2 + \eta_1^2) + P_c(\xi_2^2 + \eta_2^2) + 2\sqrt{PP_c}(\eta_1\eta_2 - \xi_1\xi_2) \right) \\
& + \frac{n\epsilon_2}{2(1-\delta)^2} \left(P(\xi_1^2 - \eta_1^2) + P_c(\xi_2^2 - \eta_2^2) - 2\sqrt{PP_c}(\eta_1\eta_2 + \xi_1\xi_2) \right) \quad (31) \\
& - \frac{n\epsilon_3}{2(1-\delta)^2} \left(\delta P(\xi_1^2 + \eta_1^2) + \left(2 - \frac{1}{\delta}\right)P_c(\xi_2^2 + \eta_2^2) + 2\delta\sqrt{PP_c}(\eta_1\eta_2 - \xi_1\xi_2) \right) \\
& + \frac{n\epsilon_4}{2(1-\delta)^2} \left(\delta P(\eta_1^2 - \xi_1^2) + \left(2 - \frac{1}{\delta}\right)P_c(\eta_2^2 - \xi_2^2) + 2\delta\sqrt{PP_c}(\eta_1\eta_2 + \xi_1\xi_2) \right).
\end{aligned}$$

This is in fact a third-order development since the powers in $(\xi_1, \xi_2, \eta_1, \eta_2)$ are even. In the forthcoming computations, this last approximation has not been used, the equations we have propagated deriving from the Hamiltonian (30).

2.3.2 The gravitational potential

To compute the gravitational potential due to the parent planet on its satellite, we must first obtain the coordinates x , y , and z of the unit vector pointing to the planet in the reference frame linked to the principal axes of inertia $(\mathbf{f}_1, \mathbf{f}_2, \mathbf{f}_3)$, from its coordinates in the inertial frame x_i , y_i and z_i . Five rotations are to be performed:

$$\begin{pmatrix} x \\ y \\ z \end{pmatrix} = R_3(-l)R_1(-J)R_3(-g)R_1(-K)R_3(-h) \begin{pmatrix} x_i \\ y_i \\ z_i \end{pmatrix} \quad (32)$$

with x_i , y_i , z_i depending on the mean longitude λ_o , the longitude of the ascending node Ω_o , the longitude of the perihelion ϖ_o , the inclination i , and the eccentricity e . The rotation matrices are defined by

$$R_3(\phi) = \begin{pmatrix} \cos \phi & -\sin \phi & 0 \\ \sin \phi & \cos \phi & 0 \\ 0 & 0 & 1 \end{pmatrix}, \quad R_1(\phi) = \begin{pmatrix} 1 & 0 & 0 \\ 0 & \cos \phi & -\sin \phi \\ 0 & \sin \phi & \cos \phi \end{pmatrix}. \quad (33)$$

The gravitational potential then reads:

$$V_1(\lambda_o, l, g, h, J, K) = -\frac{3}{2}C\frac{\mathcal{G}M_p}{d^3}(\epsilon_1(x^2 + y^2) + \epsilon_2(x^2 - y^2)) \quad (34)$$

where \mathcal{G} is the gravitational constant, M_p the mass of the perturber, i.e. Jupiter for Io, (x, y, z) the unit vector pointing at the perturber in the frame $(\mathbf{f}_1, \mathbf{f}_2, \mathbf{f}_3)$, such that $x^2 + y^2 + z^2 = 1$, while d is the distance planet-satellite.

Let us note that unlike Henrard [21], we consider that the perturbation is applied to

the whole satellite and not only to its mantle, this issue is addressed in Noyelles et al. (2010 [35]).

From the variables x , y and z , it is easy to introduce the set of variables defined in (Eq. 29). We also modify the moment Λ_o associated with λ_o (that appears in the expressions of x and y) in such way that all our variables are now canonical with multiplier $1/nC$ and our gravitational potential becomes (after division by nC)

$$\mathcal{H}_2(\lambda_o, p, P, r, R, \xi_1, \eta_1) = -\frac{3}{2} \frac{\mathcal{G}M_p}{nd^3} (\epsilon_1(x^2 + y^2) + \epsilon_2(x^2 - y^2)). \quad (35)$$

Finally, we use the formulae (30) and (35) to get the Hamiltonian of the system:

$$\mathcal{H} = \mathcal{H}_1(P, \xi_1, \eta_1, \xi_2, \eta_2) + \mathcal{H}_2(\lambda_o, p, P, r, R, \xi_1, \eta_1). \quad (36)$$

The four degrees of freedom of this Hamiltonian are the spin (p , P), the obliquity (r , R), the wobble of the whole body (ξ_1 , η_1) and the wobble of the core (ξ_2 , η_2).

2.3.3 Evaluating P_c

Since the variable p_c , spin angle of the pseudo-core, does not appear explicitly in the Hamiltonian of the system, its associated momentum P_c , norm of the angular momentum of the pseudo-core is not ruled by the Hamilton equations. So, it can be either a constant, or a time varying input as is the orbital motion of the system. We here choose to set $P_c = \delta = C_c/C$, the mean value of P being very close to 1 as our pseudo-Io is in 1:1 spin-orbit resonance. So, we assume a kind of equipartition of the norm of the angular momentum between the core and the mantle.

An exact equipartition would be $P_c(t) = \delta P(t)$, meaning that the fluid would follow every fluctuation of the orbital velocity of our pseudo-Io. It would mean that the fluid follows the longitudinal librations of the mantle, as if it were rigid. In such a case, the amplitude of the longitudinal librations would not be affected by the presence of an at least partially liquid core. Observations of such librations for Mercury (Margot et al. 2007 [29]) and the Moon (Koziel 1967 [24], Williams et al. 1973 [50]) support the assumption that the longitudinal librations are the response of the solid mantle (and not of the full body) to variations of the orbital velocity of the body. That is the reason why we consider a constant value for P_c , that results from a kind of rough averaging of P .

While this model describes the rigid dynamics of a body having a fluid core, we must not forget that real bodies on which this model could be applied have a viscous fluid core. We here discuss the relevance of our assumptions on P_c for these bodies. From a physical point of view, the reason for the decoupling between the fluid and the mantle is a low viscosity of the fluid. At the core-mantle boundary (CMB), the no-slip condition imposes that the velocity field follows the mantle. So, there is a thin turbulent layer close to this boundary, known as the Ekman layer, in which the velocity field evolves continuously from the no-slip condition at the boundary to the one satisfying $P_c = \delta$. The typical thickness of the Ekman layer is $d = \sqrt{\nu/\Omega}$ (Greenspan 1968 [17]), ν being the kinematic viscosity and $\Omega = n$ the spin frequency of the fluid. Usually a kinematic viscosity $\nu = 10^{-6} m^2/s$ is considered at the core-mantle boundary because it is consistent with a Fe/Fe-S composition (see e.g. Kerswell 1998 [23]), what yields $d = 0.16$ m. A viscosity of $36 m^2/s$ is necessary for the thickness of the Ekman layer to reach 1 km. In fact, the viscosity is expected to increase with the depth under the

CMB, since molten, and even rigid iron, should be concentrated at the inner core (see e.g. Rutter et al. [44]). We anecdotally recall the extremum of viscosity of the pitch derived from the pitch drop experiment set up in 1927 at the University of Queensland, Australia (Edgeworth et al. 1984 [12]), i.e. $\nu = (2.09 \times 10^5 \pm 4.6 \times 10^4) m^2/s$.

2.4 Link with the Navier-Stokes equation

As said in the introduction, there are at least two ways to approach the interactions between the internal structure and the rotational dynamics. One is to complexify the internal structure in considering only one degree of freedom, and the other one is to consider several dynamical degrees of freedom (4 in this study) with a quite simple internal structure. We must keep in mind that these 2 very different approaches aim at studying the same bodies. A complete study of the core dynamics would require to consider the Navier-Stokes equation, we here make a link with this equation to help in the interpretation of our model from a physical point of view.

The dynamics of a particle of fluid is often assumed to be ruled by the well-known Navier-Stokes equation, we give here its expression as given in (Greenspan 1968 [17]):

$$\frac{\partial}{\partial t} \mathbf{q} + (\mathbf{q} \cdot \nabla) \mathbf{q} + 2\boldsymbol{\Omega} \times \mathbf{q} = -\frac{1}{\rho} \nabla p - \nu \nabla \times (\nabla \times \mathbf{q}) - \mathbf{r} \times \frac{d\boldsymbol{\Omega}}{dt}, \quad (37)$$

with

- \mathbf{q} : particle velocity measured in a rotating system
- $\boldsymbol{\Omega}$: angular velocity of the rotating system, its coordinates being $(\omega_1, \omega_2, \omega_3)$
- ρ : density of the fluid
- \mathbf{r} : position of the particle
- $p = P + \rho \mathcal{U} - \frac{\rho}{2} (\boldsymbol{\Omega} \times \mathbf{r}) \cdot (\boldsymbol{\Omega} \times \mathbf{r})$: the reduced pressure, where P is the pressure of the fluid, and \mathcal{U} an exterior potential,
- ν : kinematic viscosity of the fluid.

In our case we have

$$\mathbf{q} = \begin{pmatrix} (a/c)\nu_2 x_3 - (a/b)\nu_3 x_2 \\ (b/a)\nu_3 x_1 - (b/c)\nu_1 x_3 \\ (c/b)\nu_1 x_2 - (c/a)\nu_2 x_1 \end{pmatrix}. \quad (38)$$

In an over-simplified case where we neglect the viscosity ν , the convective acceleration $(\mathbf{q} \cdot \nabla) \mathbf{q}$ and the reduced pressure p , the formula (37) reads:

$$\frac{\partial}{\partial t} \mathbf{q} + 2\boldsymbol{\Omega} \times \mathbf{q} = \mathbf{0}, \quad (39)$$

i.e.

$$\begin{aligned} \frac{d\nu_1}{dt} + 2(\omega_2 \nu_3 - \omega_3 \nu_2) &= 0, \\ \frac{d\nu_2}{dt} + 2(\omega_3 \nu_1 - \omega_1 \nu_3) &= 0, \\ \frac{d\nu_3}{dt} + 2(\omega_1 \nu_2 - \omega_2 \nu_1) &= 0. \end{aligned} \quad (40)$$

For comparison, the formula (19) reads:

$$\begin{aligned}
A \frac{d\omega_1}{dt} + D_1 \frac{d\nu_1}{dt} &= (B\omega_2 + D_2\nu_2)\omega_3 - (C\omega_3 + D_3\nu_3)\omega_2, \\
B \frac{d\omega_2}{dt} + D_2 \frac{d\nu_2}{dt} &= (C\omega_3 + D_3\nu_3)\omega_1 - (A\omega_1 + D_1\nu_1)\omega_3, \\
C \frac{d\omega_3}{dt} + D_3 \frac{d\nu_3}{dt} &= (A\omega_1 + D_1\nu_1)\omega_2 - (B\omega_2 + D_2\nu_2)\omega_1.
\end{aligned} \tag{41}$$

The systems of equations (40) and (41) present some similarities, the main difference being that the moments of inertia are involved in Eq.41. They should be in fact considered as global equations (i.e. considering the whole volume of fluid), while the Eq.40 is a local form, considering an individual fluid particle.

The reader can find another formulation of these equations in (Rambaux et al. 2007 [40]).

3 A numerical study

3.1 The algorithm

As shown in Henrard [21], the proper frequency associated with the core, i.e. the free core nutation, is close to the spin period of the considered body. For a synchronous satellite, this period is also the orbital period, so we have a proximity between a proper frequency of the problem and a forcing period. As a consequence, a perturbative approach will meet difficulties to converge because of small divisors. Such a problem has already been encountered in (Noyelles et al. 2010 [35]). That is the reason why we prefer a full numerical study, consisting of a numerical integration of the equations derived from the Hamiltonian (36), and a frequency analysis of the solutions of the problem. The frequency analysis algorithm we use is widely inspired from NAFF (see Laskar 1993 [26] for the method, and Laskar 2005 [27] for the convergence proofs), with a refinement suggested by Champenois (1998 [5]) consisting in iterating the process to enhance the accuracy of the determination.

The basic idea of the frequency analysis is to consider that a complex variable of the problem $x(t)$ is quasi-periodic, i.e. can be expressed as a, a priori infinite, sum of a converging trigonometric series like

$$x(t) = \sum_{n=0}^{\infty} A_n \exp(i\nu_n t) \tag{42}$$

where A_n are constant complex amplitudes, and ν_n constant frequencies, with

$$x(t) \approx \sum_{n=0}^N A_n^\bullet \exp(i\nu_n^\bullet t), \tag{43}$$

the bullet meaning that the coefficients have been numerically determined. A detailed description of the algorithm is given in appendix. In the case of a real variable, the Eq.43 becomes

$$x(t) \approx \sum_{n=0}^N A_n^\bullet \cos(\nu_n^\bullet t + \phi_n^\bullet), \quad (44)$$

or

$$x(t) \approx \sum_{n=0}^N A_n^\bullet \sin(\nu_n^\bullet t + \phi_n^\bullet), \quad (45)$$

where the amplitudes are now real, and the ϕ_n^\bullet are real phases expressed with the counterclockwise convention, previously included in the complex amplitudes.

The rotation of a synchronous satellite is reputed to have reached an equilibrium state, known as Cassini State 1 (see e.g. Cassini 1693 [4], Peale 1969 [37], and Bouquillon et al. 2003 [3] for an extension to the polar motion), after dissipation of its rotational energy. There should remain free oscillations with negligible amplitude around the equilibrium, in the following we assume them as null, since they cannot be detected except for the Moon (Rambaux & Williams 2011 [42]). It can be shown that, for rigid dynamics, between 2 and 4 Cassini States exist. In the context of natural satellites of the giant planets where the nodal precession rate is small with respect to the orbital frequency, the 4 Cassini States exist, and they induce an obliquity close to $k\frac{\pi}{2}$, k being an integer (see Ward & Hamilton 2004 [49] or Noyelles 2010 [34], Appendix B). The Cassini State 1, corresponding to $k = 0$, i.e. a small obliquity, is a priori the most probable one, because it is stable and the primordial obliquity of the satellite is thought to be small.

In order to numerically simulate the rotational dynamics of the satellite, we need initial conditions that are actually very close to the equilibrium, that is perturbed by the orbital dynamics of the satellite. For that, we use the algorithm NAFFO (Noyelles et al. 2011 [36]), consisting in:

1. A first numerical integration of the equations of the system, with initial conditions conveniently chosen,
2. Frequency analysis of the solution and identification of the contributions depending on the free modes,
3. Evaluation of the free modes at the time origin of the numerical simulation, and removal from the initial conditions,

then the process is iterated until convergence. In a Hamiltonian framework as is the case here, Noyelles et al. [36] have shown that the convergence is quadratic in the amplitude of the free modes, provided that the quasi-periodic decomposition is exact, i.e. that the signal is indeed quasi-periodic, and that the numerical error has negligible impact. The proof is based on the d'Alembert characteristic (see e.g. Henrard 1974 [18]), that gives a relation between the amplitudes A_n and the arguments $\nu_n t$ in Eq.43. This algorithm has already been successfully applied in problem of rotational dynamics (Dufey et al. 2009 [11], Noyelles 2009 [33], Robutel et al. 2011 [43]), in dynamics of exoplanetary systems (Couetdic et al. 2010 [8]), and in the analysis of ground-track resonances around Vesta (Delsate 2011 [9]).

3.2 The numerical tests

The numerical algorithm we have just described has been used in different cases, dependent on the free parameters ϵ_3 , ϵ_4 (\approx polar flattening and equatorial ellipticity of

Table 1 Physical and dynamical parameters ruling our pseudo-Io. We used the same as [21]. The orbital frequency n and the regression rate of the ascending orbital node $\dot{\Omega}$ are taken from L1.2 ephemerides [25]. The phases (initial conditions of the orbital angles) are arbitrarily chosen.

Parameter	Value
GM_p (planet)	$1.261648547674763616 \times 10^{23} \text{ km}^3 \cdot \text{s}^{-2}$
GM (satellite)	$5955.5 \text{ km}^3 \cdot \text{s}^{-2}$
R_p	71492 km
J_{2p}	1.4736×10^{-2}
J_2	1.828×10^{-3}
C_{22}	5.537×10^{-4}
$C/(MR^2)$	0.376856
a	422029.958 km
e	4.15×10^{-3}
I	2.16 arcmin
n	1297.2044725279755 rad/y
$\dot{\varpi}$	0.97311853791375 rad/y
$\dot{\Omega}$	$-0.8455888497945 \text{ rad/y}$
$\lambda_o(0)$	0
$\varpi_o(0)$	2 rad
$\delta\lambda_o(0)$	0.1 rad
$\epsilon_1 = J_2 \frac{MR^2}{C}$	4.85066×10^{-3}
$\epsilon_2 = 2C_{22} \frac{MR^2}{C}$	2.93852×10^{-3}

the core), and $\delta = C_c/C$, representing the size of the core through its inertial polar momentum. In all our simulations we considered a kind of pseudo-Io, i.e. a satellite with physical and dynamical properties close to the ones of the Galilean satellite of Jupiter Io, except that its orbit has constant eccentricity and inclination. The numerical integrations are performed with the Adams-Bashforth-Moulton 10th order predictor-corrector integrator, with a tolerance of 10^{-14} , and a step size of $5 \times 10^{-5} \text{ y} \approx 1.8 \times 10^{-3} \text{ d}$.

We considered as reference values for the internal structure parameters $\delta = 0.5$, $\epsilon_3 = \epsilon_1$ and $\epsilon_4 = \epsilon_2$, and we tested different pseudo-Ios with different values of these parameters.

4 “Classical” behavior

We expect to have, at the Cassini State 1:

- $\sigma = p - \lambda_o + \pi$ close to 0 because of the 1:1 spin-orbit resonance,
- P close to 1 (the norm of the angular momentum being close to nC),
- $\rho = \delta\lambda_o - h = \delta\lambda_o + r$ (third Cassini Law),
- R close to 0 (the obliquity being small),
- J and J_c close to 0 (small polar motions of the satellite and its core),

the “classical” behavior being small oscillations around this equilibrium. We use it to define our first initial conditions, before refining them with NAFFO.

Table 2 Proper frequencies of the small oscillations around the equilibrium for $\epsilon_3 = \epsilon_1$, $\epsilon_2 = \epsilon_4$ and $\delta = 0.5$. n is the orbital frequency given in Tab.1.

	Frequency (rad/y)	Period (d)	ω/n
ω_u	243.4050908	9.42845	0.187638
ω_v	4.1898509	547.73630	3.2299×10^{-3}
ω_w	19.5319416	117.49643	0.015057
ω_z	1334.4264821	1.71979	1.028694

Table 3 The variable P-1. The series are in cosine.

	Amplitude	Frequency (rad/y)	Phase (t=0)	T (d)	Identification
1	1.5156914×10^{-4}	1296.2313540	65.408°	1.77047	$\lambda_o - \varpi_o + \pi$
2	6.6760683×10^{-7}	2592.4627080	-49.183°	0.88523	$2\lambda_o - 2\varpi_o + \pi$
3	3.8653845×10^{-9}	3888.6940620	-163.775°	0.59016	$3\lambda_o - 3\varpi_o + \pi$
4	1.2702319×10^{-9}	0	-180°	∞	cst
5	$2.2957822 \times 10^{-11}$	5184.9254160	81.634°	0.44262	$4\lambda_o - 4\varpi_o + \pi$
6	$1.5952860 \times 10^{-11}$	2596.1001228	-11.459°	0.88399	$2\lambda_o - 2\varrho$

4.1 In-depth study of a reference case

We here present an in-depth study of a “reference case”, considering $\epsilon_3 = \epsilon_1$, $\epsilon_4 = \epsilon_2$, and $\delta = 0.5$. This study consists of a numerical estimation of the frequencies of the proper librations (Tab.2), and of a numerical decomposition of the canonical variables (Tab.3 to 8).

We recall that the orbital frequency n is 1297.20447137 rad/y (Lainey et al. 2006 [25]). A comparison with Henrard [21] lacks of significance since the physical model was different (the gravitational torque of Jupiter acting only on the mantle, while it acts on the whole satellite here), but we can see that, like Henrard, we find a proper frequency of the core ω_z close to the spin frequency of Io, that is also its orbital frequency since our satellite is locked in the 1:1 spin-orbit resonance.

The Tab.3 to 8 give a quasi-periodic decomposition of the canonical variables with identification of the forced oscillations, i.e. the mean longitude of our pseudo-Io λ_o , the motion of its pericenter ϖ_o , and the motion of its orbital ascending node ϱ_o . The phases are indicated at the time origin and allow to determine the presence of π or $\pi/2$ in the identification.

Since our rotational model takes 4 degrees of freedom into account, we can split the canonical variables and moments into 3 groups related to these degrees of freedom.

The first group (σ, P) (Tab.3 & 4) can be linked to the longitudinal motion. We can see that the mean position is the theoretical equilibrium ($\sigma = 0, P = 1$) related to the 1:1 spin-orbit resonance, and there are small oscillations around this equilibrium, related to the mean anomaly $\lambda_o - \varpi_o$ and its harmonics. We can see from the Tab.4 that the deviation from the theoretical equilibrium does not exceed 2 arcmin for an eccentricity of 4.15×10^{-3} . This amplitude is proportional to the eccentricity (at least for small eccentricities, see e.g. Comstock & Bills 2003 [7]), that induces periodic variations of the planet-satellite distance.

The second group (ρ, R) (Tab.5 & 6) locates the angular momentum of the whole body with respect to the orbital plane. Once more, the angle can be averaged to 0 with a instantaneous departure that does not exceed 2 arcmin, this equilibrium is a consequence of the third Cassini law. It is also known that the mean obliquity, that can

Table 4 The resonant argument σ . The series are in cosine.

	Amplitude	Frequency (rad/y)	Phase (t=0)	T (d)	Identification
1	62.574 arcsec	1296.2313540	-24.592°	1.77047	$\lambda_o - \varpi_o + \pi/2$
2	0.138 arcsec	2592.4627080	-139.183°	0.88523	$2\lambda_o - 2\varpi_o + \pi/2$
3	0.053 arcsec	3888.6940620	106.225°	0.59016	$3\lambda_o - 3\varpi_o + \pi/2$
4	2.03×10^{-5} arcsec	2596.1001228	-101.459°	0.88399	$2\lambda_o - 2\varrho_o - \pi/2$
5	2.37×10^{-6} arcsec	5184.9254164	-8.366°	0.44262	$4\lambda_o - 4\varpi_o + \pi/2$
6	1.21×10^{-6} arcsec	1299.8687682	166.868°	1.76551	$\lambda_o + \varpi_o - 2\varrho_o - \pi/2$

Table 5 The variable R . The series are in cosine.

	Amplitude	Frequency (rad/y)	Phase (t=0)	T (d)	Identification
1	2.5966515×10^{-7}	0	0°	∞	cst
2	$1.6920424 \times 10^{-10}$	2596.1001228	-11.459°	0.88399	$2\lambda_o - 2\varrho_o$
3	$3.1006440 \times 10^{-11}$	1296.2313540	65.408°	1.77047	$\lambda_o - \varpi_o + \pi$
4	$1.2914058 \times 10^{-12}$	3892.3314767	-36.051°	0.58960	$3\lambda_o - \varpi_o - 2\varrho_o + \pi/2$
5	$5.5914871 \times 10^{-13}$	3.6374149	-142.276°	630.924	$2\varpi_o - 2\varrho_o$

Table 6 The variable ρ . The series are in cosine.

	Amplitude	Frequency (rad/y)	Phase (t=0)	T (d)	Identification
1	67.204 arcsec	2596.1001228	78.541°	0.88399	$2\lambda_o - 2\varrho_o + \pi/2$
2	1.542 arcsec	1296.2313540	155.408°	1.77047	$\lambda_o - \varpi_o - \pi/2$
3	0.517 arcsec	3892.3314767	53.949°	0.58960	$3\lambda_o - \varpi_o - 2\varrho_o + \pi$
4	0.222 arcsec	3.6374146	-52.276°	630.924	$2\varpi_o - 2\varrho_o - 3\pi/2$

Table 7 The variable $\eta_1 + \nu\xi_1$. The series are in complex exponential.

	Amplitude	Frequency (rad/y)	Phase (t=0)	T (d)	Identification
1	5.22646×10^{-5}	-1298.0500614	-174.270°	1.76799	$-\lambda_o + \varrho_o - \pi$
2	5.54231×10^{-7}	1298.0500614	174.270°	1.76799	$\lambda_o - \varrho_o + \pi$
3	2.81640×10^{-7}	-1.8187074	71.138°	1261.849	$\varrho_o - \varpi_o + \pi$
4	2.20597×10^{-7}	1.8187074	-71.138°	1261.849	$\varpi_o - \varrho_o - \pi$
5	5.96421×10^{-9}	-2594.2814154	-59.679°	0.88461	$\varpi_o + \varrho_o - 2\lambda_o - \pi$
6	3.66084×10^{-9}	2594.2814154	59.679°	0.88461	$2\lambda_o - \varpi_o - \varrho_o + \pi$

be derived from the mean value of R , is due to the interior structure and the regression rate of the orbital node (see e.g. Ward & Hamilton 2004 [49]). We can also see that the oscillations are dominated by the mode $2\lambda_o - 2\varrho_o$, emphasizing an influence of the orbital node on this degree of freedom.

The third group involves the last two degrees of freedom (ξ_1, η_1) (Tab.7) and (ξ_2, η_2) (Tab.8), that are strongly coupled as shown by Henrard [21]). They represent respectively the polar motion of the whole body and the orientation of the velocity field of the fluid. They are ruled by two kinds of small oscillations: fast ones due to harmonics of the proper mode $\lambda_o - \varrho_o$, and slow ones due to the argument of the pericenter $\varpi_o - \varrho_o$.

Table 8 The variable $\eta_2 + i\xi_2$. The series are in complex exponential.

	Amplitude	Frequency (rad/y)	Phase (t=0)	T (d)	Identification
1	7.36054×10^{-5}	1298.0500614	-5.730°	1.76799	$\lambda_o - \delta\Omega_o$
2	3.33184×10^{-7}	-1298.0500614	5.730°	1.76799	$-\lambda_o + \delta\Omega_o$
3	2.03442×10^{-7}	1.8187074	108.862°	1261.849	$\varpi_o - \delta\Omega_o$
4	1.55904×10^{-7}	-1.8187074	-108.862°	1261.849	$\delta\Omega_o - \varpi_o$

Table 9 Influence of the size of the core δ , with $\epsilon_3 = \epsilon_1$ and $\epsilon_4 = \epsilon_2$.

δ	T_u (d)	T_v (d)	T_w (d)	T_z (d)	R^*
0.1	12.650	453.259	208.551	1.745	2.304×10^{-7}
0.2	11.926	480.369	185.790	1.741	2.365×10^{-7}
0.3	11.156	504.669	163.028	1.736	2.450×10^{-7}
0.4	10.328	526.965	140.264	1.729	2.525×10^{-7}
0.5	9.428	547.734	117.496	1.720	2.597×10^{-7}
0.6	8.433	567.278	94.723	1.706	2.680×10^{-7}
0.7	7.303	585.780	71.939	1.685	2.760×10^{-7}
0.8	5.963	603.294	49.130	1.645	2.842×10^{-7}
0.9	4.216	619.394	26.230	1.540	2.922×10^{-7}

Table 10 Influence of the polar flattening of the core ϵ_3 , with $\delta = 0.5$ and $\epsilon_4 = \epsilon_2$.

ϵ_3/ϵ_1	T_u (d)	T_v (d)	T_w (d)	T_z (d)	R^*
0.2	9.428	6414.819	117.118	1.728	1.040×10^{-6}
0.3	9.428	2491.673	117.112	1.727	4.612×10^{-7}
0.4	9.428	1572.784	117.121	1.726	3.592×10^{-7}
0.5	9.428	1163.452	117.147	1.725	3.177×10^{-7}
1	9.428	547.734	117.496	1.720	2.597×10^{-7}
3	9.428	254.876	122.879	1.695	2.326×10^{-7}
5	9.428	210.742	136.657	1.668	2.277×10^{-7}
6	9.428	200.875	148.926	1.655	2.268×10^{-7}
7	9.428	194.454	168.492	1.641	2.260×10^{-7}
8	9.428	189.284	201.639	1.628	2.256×10^{-7}
9	9.428	185.621	278.943	1.616	2.251×10^{-7}

4.2 Influence of the parameters

To characterise the influence of the internal structure parameters (i.e. ϵ_3 , ϵ_4 and δ), we quantify their effects on our outputs. We choose here to consider in particular the proper frequencies ω_u to ω_z , and the mean value of R (Tab.9 to 11).

We can see that all these outputs depend on the size of the core δ (Tab.9). In particular, the period of the free longitudinal librations T_u follows the classical law (see e.g. Goldreich & Peale 1966 [16]):

$$T_u \approx \frac{\pi}{n} \sqrt{\frac{C_m / (MR^2)}{3C_{22}}}, \quad (46)$$

yielding $T_u \propto \sqrt{1-\delta}$. We note that this period depends on the size of the core, while Henrard did not find any dependency in applying the gravitational torque just on the mantle. To check the influence of the shape of the core, we now present the outputs with varying ϵ_3 (Tab.10) and ϵ_4 (Tab.11).

We recall that for Mercury, i.e. in the case of the 3:2 spin-orbit resonance, the flattening of the core ϵ_3 alters the frequencies ω_v and ω_z , but not the others ones.

Table 11 Influence of the equatorial ellipticity of the core ϵ_4 , with $\delta = 0.5$ and $\epsilon_3 = \epsilon_1$.

ϵ_4/ϵ_2	T_u (d)	T_v (d)	T_w (d)	T_z (d)	R^*
0	9.428	545.949	117.771	1.7199	2.5996×10^{-7}
0.1	9.428	546.128	117.718	1.7199	2.5998×10^{-7}
0.5	9.428	546.841	117.563	1.7199	2.5954×10^{-7}
1	9.428	547.734	117.496	1.7198	2.5967×10^{-7}
3	9.428	551.316	118.652	1.7195	2.6070×10^{-7}
5	9.428	554.914	122.283	1.7193	2.6069×10^{-7}
10	9.428	564.010	149.248	1.7186	2.6248×10^{-7}

Here, the variations of the period of the free longitudinal librations T_u have only negligible variations, while the 3 other proper frequencies are affected. As for Mercury, the periods T_v and T_z increase with ϵ_3 getting closer to 0, T_z getting closer to the spin period 1.769 d, and T_v tending to infinity. We also have an increase of the free wobble period when ϵ_3 increases. We can note that it seems to be possible to fine-tune the parameters ($\epsilon_3 \approx 7.7\epsilon_1$) to have a resonance between the free wobble and the free oscillations of the obliquity ($T_v = T_w$), but this is only anecdotal. This very peculiar case would require strict fine-tuning between the flattening of the body and of the core to occur, so we can consider it as very unlikely. Finally, the equilibrium position of the angular momentum, i.e. R^* , is shifted from the origin (here the normal to the orbit) when the core tends to be spherical (small ϵ_3).

In the case of the 3:2 spin-orbit resonance, no significant influence of the equatorial ellipticity of the core had been detected. We here (Tab.11) see a small influence on T_v , T_w , T_z and R^* , but that does not seem to be significant. Once more, the longitudinal librations seem not to be affected.

As a reminder, Henrard [19] found free periods of respectively $T_u = 13.25$, $T_v = 159.39$ and $T_w = 229.85$ days in considering a rigid Io. The rigid value of 13.25 days can be obtained in setting $C_m = C$ in Eq.46.

5 Analysis of a bifurcation

In the previous section, we do not present the behavior of the system for some physically possible values of the core shape parameters ϵ_3 and ϵ_4 . The reason is that for some range of these parameters, the system presents more complex behaviors, that we here introduce. In particular, we assume since the beginning a “classical” Cassini State 1 in which null amplitudes of the polar motions of the body J and of the core J_c define a stable equilibrium. In fact, this has not been checked yet, and our numerical investigations have revealed that this equilibrium is unstable for instance for $\delta = 0.5$, $\epsilon_3 = 10\epsilon_1$ and $\epsilon_4 = 0$.

5.1 Numerical characterisation of the equilibria

A simulation of the behavior of the system for $\delta = 0.5$, $\epsilon_3 = 10\epsilon_1$ and $\epsilon_4 = 0$ gives a butterfly shape for the outputs related to the polar motion of the body (η_1, ξ_1) and of the velocity field of the fluid (η_2, ξ_2) for the solution passing close to the equilibrium defined by $J = J_c = 0$ (Fig.3). It suggests that this equilibrium is in fact unstable, and that two new stable equilibria appear.

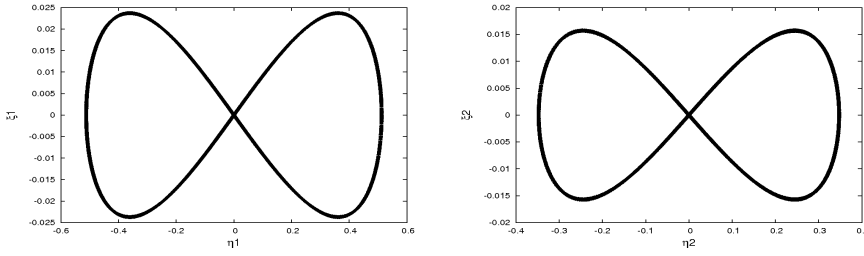


Fig. 3 Trajectory passing close to the equilibrium $\xi_1 = \xi_2 = \eta_1 = \eta_2$ for $\delta = 0.5$, $\epsilon_3 = 10\epsilon_1$ and $\epsilon_4 = 0$. The left panel shows the polar motion of the whole body, and the right one is related to the pseudo-core. We can see that the trajectory does not librate around this equilibrium, but presents a butterfly-shape, that suggests the presence of 2 new stable equilibria.

Table 12 The variable P-1 for $\epsilon_3 = 10\epsilon_1$ and $\epsilon_4 = 0$. The series are in cosine.

	Amplitude	Frequency (rad/y)	Phase (t=0)	T (d)	Identification
1	2.81032×10^{-3}	0	0	∞	cst
2	1.56939×10^{-4}	1296.2313540	65.408°	1.77047	$\lambda_o - \varpi_o + \pi$
3	6.77223×10^{-7}	2592.4627080	-49.183°	0.88523	$2\lambda_o - 2\varpi_o + \pi$
4	5.20072×10^{-8}	1298.0500614	174.270°	1.76799	$\lambda_o - \delta\Omega_o + \pi$
5	3.80792×10^{-8}	1.8187074	288.862°	1261.849	$\varpi_o - \delta\Omega_o + \pi$
6	3.92165×10^{-9}	3888.6940620	-163.775°	0.59016	$3\lambda_o - 3\varpi_o + \pi$
7	3.50511×10^{-10}	2594.2814154	59.679°	0.88461	$2\lambda_o - \varpi_o - \delta\Omega_o + \pi$

Table 13 The resonant argument σ for $\epsilon_3 = 10\epsilon_1$ and $\epsilon_4 = 0$. The series are in cosine.

	Amplitude	Frequency (rad/y)	Phase (t=0)	T (d)	Identification
1	63.973 arcsec	1296.2313540	-24.592°	1.77047	$\lambda_o - \varpi_o + \pi/2$
2	0.139 arcsec	2592.4627080	-139.183°	0.88523	$2\lambda_o - 2\varpi_o + \pi/2$
3	0.113 arcsec	1298.0500614	84.270°	1.76799	$\lambda_o - \delta\Omega_o + \pi/2$
4	5.4×10^{-4} arcsec	3888.6940620	106.225°	0.59016	$3\lambda_o - 3\varpi_o + \pi/2$
5	3.0×10^{-5} arcsec	2594.2814154	149.679°	0.88461	$2\lambda_o - \varpi_o - \delta\Omega_o + 3\pi/2$
6	2.2×10^{-5} arcsec	1294.4126466	46.546°	1.77295	$\lambda_o - 2\varpi_o + \delta\Omega_o + 3\pi/2$
7	1.6×10^{-5} arcsec	2596.1001228	-101.459°	0.88399	$2\lambda_o - 2\delta\Omega_o - \pi/2$

These equilibria have been reached thanks to NAFFO. The quasi-periodic decompositions of the solution corresponding to the equilibrium ($\xi_1 = \xi_2 = 0, \eta_1 \approx 0.25, \eta_2 \approx -0.17$) are given in Tab.12 to 17. The other equilibrium is symmetrical to this one, i.e. corresponds to ($\xi_1 = \xi_2 = 0, \eta_1 \approx -0.25, \eta_2 \approx 0.17$).

We can see from these tables that the difference is not only in $(\xi_1, \eta_1, \xi_2, \eta_2)$. The difference for the degree of freedom related to the longitudinal behavior (σ, P) is striking. First, we can see a significant departure (2.81×10^{-3}) from the expected mean P, i.e. 1 (Tab.12). We also note significant longitudinal librations related to the combination of proper modes $\lambda_o - \delta\Omega_o$ (Tab.13), that did not appear in the “classical” behavior (Tab.4).

The difference is even more important for the degree of freedom related to the location of the angular momentum, i.e. (ρ, R) (Tab.15 & 14). In this case, we can see large oscillations associated with the argument of the pericenter $\varpi_o - \delta\Omega_o$. It is known that a motion due to the position of the pericenter has the eccentricity as physical

Table 14 The variable R for $\epsilon_3 = 10\epsilon_1$ and $\epsilon_4 = 0$. The series are in cosine.

	Amplitude	Frequency (rad/y)	Phase (t=0) ($^\circ$)	T (d)	Identification
1	3.3172485×10^{-7}	0	0°	∞	cst
2	3.0899861×10^{-7}	1.8187074	108.862°	1261.849	$\varpi_o - \delta_{\Omega_o}$
3	$1.4728954 \times 10^{-10}$	2596.1001228	-11.459°	0.88399	$2\lambda_o - 2\delta_{\Omega_o}$
4	$7.9302319 \times 10^{-11}$	2592.4627080	-49.183°	0.87986	$2\lambda_o - 2\varpi_o + \pi$
5	$2.0015617 \times 10^{-11}$	1296.2313540	65.408°	1.77047	$\lambda_o - \varpi_o + \pi$
6	$1.5218917 \times 10^{-11}$	2594.2814154	-120.321°	0.88461	$2\lambda_o - \varpi_o - \delta_{\Omega_o}$
7	$8.1094453 \times 10^{-12}$	1294.4126466	46.546°	1.77295	$\lambda_o - 2\varpi_o + \delta_{\Omega_o} + 3\pi/2$
8	$4.4761150 \times 10^{-12}$	1298.0500614	174.270°	1.76799	$\lambda_o - \delta_{\Omega_o} + \pi$

Table 15 The variable ρ for $\epsilon_3 = 10\epsilon_1$ and $\epsilon_4 = 0$. The series are in cosine.

	Amplitude	Frequency (rad/y)	Phase (t=0) ($^\circ$)	T (d)	Identification
1	39.163°	1.8187074	18.862°	1261.849	$\varpi_o - \delta_{\Omega_o} - \pi/2$
2	13.384°	3.6374148	127.724°	630.924	$2\varpi_o - 2\delta_{\Omega_o} - \pi/2$
3	6.099°	5.4561222	-123.414°	420.616	$3\varpi_o - 3\delta_{\Omega_o} - \pi/2$
4	3.127°	7.2748300	-14.552°	315.462	$4\varpi_o - 4\delta_{\Omega_o} - \pi/2$
5	1.710°	9.0935369	94.310°	252.370	$5\varpi_o - 5\delta_{\Omega_o} - \pi/2$
6	58.431 arcmin	10.9122443	-156.828°	210.308	$6\varpi_o - 6\delta_{\Omega_o} - \pi/2$
7	34.233 arcmin	12.7309517	-47.966°	180.264	$7\varpi_o - 7\delta_{\Omega_o} - \pi/2$
8	20.474 arcmin	14.5496590	60.896°	157.731	$8\varpi_o - 8\delta_{\Omega_o} - \pi/2$
9	12.440 arcmin	16.3683661	169.758°	140.205	$9\varpi_o - 9\delta_{\Omega_o} - \pi/2$
10	7.653 arcmin	18.1870733	-81.380°	126.185	$10\varpi_o - 10\delta_{\Omega_o} - \pi/2$
11	4.755 arcmin	20.0057804	27.482°	114.714	$11\varpi_o - 11\delta_{\Omega_o} - \pi/2$
12	2.979 arcmin	21.8244872	136.344°	105.154	$12\varpi_o - 12\delta_{\Omega_o} - \pi/2$
13	1.880 arcmin	23.6431936	-114.794°	97.065	$13\varpi_o - 13\delta_{\Omega_o} - \pi/2$
14	1.715 arcmin	2596.1001226	78.541°	0.88399	$2\lambda_o - 2\delta_{\Omega_o} + \pi/2$
15	1.193 arcmin	25.4618992	-5.932°	90.132	$14\varpi_o - 14\delta_{\Omega_o} - \pi/2$
16	1.168 arcmin	2597.9188300	-172.597°	0.88337	$2\lambda_o + \varpi_o - 3\delta_{\Omega_o} - 3\pi/2$
17	52.836 arcsec	2594.2814149	-30.321°	0.88461	$2\lambda_o - \varpi_o - \delta_{\Omega_o} - 3\pi/2$
18	47.694 arcsec	2599.7375373	-116.265°	0.88276	$2\lambda_o + 2\varpi_o - 4\delta_{\Omega_o} - 3\pi/2$
19	45.673 arcsec	27.2806037	102.930°	84.123	$15\varpi_o - 15\delta_{\Omega_o} - \pi/2$
20	32.468 arcsec	2601.5562447	45.127°	0.88214	$2\lambda_o + 3\varpi_o - 5\delta_{\Omega_o} - 3\pi/2$
21	29.268 arcsec	29.0993068	-148.208°	78.866	$16\varpi_o - 16\delta_{\Omega_o} - \pi/2$
22	22.103 arcsec	2603.3749520	153.989°	0.88152	$2\lambda_o + 4\varpi_o - 6\delta_{\Omega_o} - 3\pi/2$
23	18.829 arcsec	30.9180086	-39.346°	74.226	$17\varpi_o - 17\delta_{\Omega_o} - \pi/2$
24	15.046 arcsec	2605.1936596	-97.149°	0.88091	$2\lambda_o + 5\varpi_o - 7\delta_{\Omega_o} - 3\pi/2$

Table 16 The variable $\eta_1 + i\xi_1$ for $\epsilon_3 = 10\epsilon_1$. The series are in complex exponential.

	Amplitude	Frequency (rad/y)	Phase (t=0) ($^\circ$)	T (d)	Identification
1	0.2501568	0	0°	∞	cst
2	3.36571×10^{-5}	-1296.2313540	-155.408°	1.77047	$\varpi_o - \lambda_o - 3\pi/2$
3	7.44538×10^{-6}	1296.2313540	155.408°	1.77047	$\lambda_o - \varpi_o + 3\pi/2$
4	5.19058×10^{-6}	-1298.0500614	-174.270°	1.76799	$-\lambda_o + \delta_{\Omega_o} - \pi$
5	1.72624×10^{-6}	1.8187074	-71.138°	1261.849	$\varpi_o - \delta_{\Omega_o} + \pi$
6	1.69988×10^{-6}	-1.8187074	71.138°	1261.849	$\delta_{\Omega_o} - \varpi_o - \pi$
7	5.90500×10^{-7}	1298.0500614	174.270°	1.76799	$\lambda_o - \delta_{\Omega_o} + \pi$
8	4.69722×10^{-8}	2592.4627080	-49.183°	0.88523	$2\lambda_o - 2\varpi_o + \pi$
9	3.95648×10^{-8}	-2592.4627080	43.183°	0.88523	$2\varpi_o - 2\lambda_o - \pi$
10	3.31650×10^{-9}	2594.2814161	59.679°	0.88461	$2\lambda_o - \varpi_o - \delta_{\Omega_o} + \pi$

Table 17 The variable $\eta_2 + i\xi_2$ for $\epsilon_3 = 10\epsilon_1$. The series are in complex exponential.

	Amplitude	Frequency (rad/y)	Phase (t=0) ($^\circ$)	T (d)	Identification
1	0.1690165	0	180°	∞	cst
2	3.25350×10^{-5}	1296.2313540	-114.592°	1.77047	$\lambda_o - \varpi_o$
3	7.01986×10^{-6}	1298.0500614	-5.730°	1.76799	$\lambda_o - \varOmega_o$
4	1.16880×10^{-6}	-1.8187074	-108.862°	1261.848	$\varOmega_o - \varpi_o$
5	1.15291×10^{-6}	1.8187074	108.862°	1261.848	$\varpi_o - \varOmega_o$
6	1.09791×10^{-6}	-1296.2313540	-65.408°	1.77047	$\varpi_o - \lambda_o - \pi$
7	2.37221×10^{-7}	-1298.0500614	5.730°	1.76799	$\varOmega_o - \lambda_o$
8	8.29840×10^{-9}	2592.4627079	130.817°	0.88523	$2\lambda_o - 2\varpi_o$
9	4.26308×10^{-9}	2594.2814150	59.679°	0.88461	$2\lambda_o - \varpi_o - \varOmega_o + \pi$
10	1.54598×10^{-9}	-2592.4627077	-130.817°	0.88523	$2\varpi_o - 2\lambda_o$

cause, while our eccentricity is only 4.15×10^{-3} , the peak-to-peak oscillations of ρ reaching 80° . So, we can expect higher oscillations for bigger eccentricities.

In this case, the shift of P led us to change iteratively the value of the constant P_c so that it remains equal to $\delta < P >$. We have seen that a change of P_c yields a significant difference on the locations of the stable equilibria, that is the reason why the mean values of $\eta_1 + i\xi_1$ and $\eta_2 + i\xi_2$ we give in Tab.16,17 are significantly different from the ones that can be guessed from Fig.3.

5.2 Analytical study

In order to understand the appearance of 2 new stable equilibria, we propose a simplified analytical study of the problem. This study consists in starting from the Hamiltonian \mathcal{H} (Eq.36), in expressing the oscillating angle (respectively $\sigma = p - \lambda_o + \pi$ because of the 1:1 spin-orbit resonance, and $\rho = \varOmega_o - h$ because of the third Cassini Law), in averaging over the circulating ones, to deduce a secular Hamiltonian yielding the equilibria. All these calculations have been performed thanks to Maple software.

The starting point is the Hamiltonian \mathcal{H} (Eq.36) in which the coordinates of the perturber (i.e. a pseudo-Jupiter if we consider a pseudo-Io) x and y are replaced thanks to Eq.32 with

$$x_i = -(\cos \varOmega_o \cos(\lambda_o - \varOmega_o) - \cos I_o \sin \varOmega_o \sin(\lambda_o - \varOmega_o)), \quad (47)$$

$$y_i = -(\sin \varOmega_o \cos(\lambda_o - \varOmega_o) + \cos I_o \cos \varOmega_o \sin(\lambda_o - \varOmega_o)), \quad (48)$$

$$z_i = -\sin I_o \sin(\lambda_o - \varOmega_o). \quad (49)$$

We here neglect the influence of the eccentricity.

Then the following canonical transformation is performed

$$\begin{aligned} \sigma &= p - \lambda_o + \pi, & P, \\ \rho &= \varOmega_o + r, & R, \\ \xi_1, & & \eta_1, \\ \xi_2, & & \eta_2. \end{aligned} \quad (50)$$

Since this transformation, involving λ_o and \varOmega_o , is time-dependent, we must add $-nP + \dot{\varOmega}R$ to the Hamiltonian. σ and ρ are oscillating arguments that can be averaged to 0, while λ_o and \varOmega_o are circulating.

A first-order averaging of the Hamiltonian is performed, then the Hamilton equations are derived, i.e.

$$\begin{aligned}
\frac{d\sigma}{dt} &= \frac{\partial \mathcal{H}}{\partial P}, & \frac{dP}{dt} &= -\frac{\partial \mathcal{H}}{\partial \sigma}, \\
\frac{d\rho}{dt} &= \frac{\partial \mathcal{H}}{\partial R}, & \frac{dR}{dt} &= -\frac{\partial \mathcal{H}}{\partial r}, \\
\frac{d\xi_1}{dt} &= \frac{\partial \mathcal{H}}{\partial \eta_1}, & \frac{d\eta_1}{dt} &= -\frac{\partial \mathcal{H}}{\partial \xi_1}, \\
\frac{d\xi_2}{dt} &= \frac{\partial \mathcal{H}}{\partial \eta_2}, & \frac{d\eta_2}{dt} &= -\frac{\partial \mathcal{H}}{\partial \xi_2},
\end{aligned} \tag{51}$$

the equilibria corresponding to null time derivatives of the variables and associated moments, i.e. the right-hand side of these equations vanish. The numerical exploration drove us to neglect the influence of the inclination and the obliquity ($I = 0$, $R = 0$), and to consider ξ_1 and ξ_2 as null at the equilibrium. These approximations allowed us to simplify the system, and we finally find with a good agreement the equilibrium values of P , η_1 and η_2 in solving numerically the following equations:

$$\begin{aligned}
\frac{1}{n} \frac{d\sigma}{dt} &= -1 + \frac{P - P_c}{1 - \delta} + \frac{\eta_1^2}{2(1 - \delta)^2} (\epsilon_1 - \epsilon_2 - \delta\epsilon_3 + \delta\epsilon_4) + \frac{\eta_2^2}{2(1 - \delta)} \\
&+ \frac{\eta_1 \eta_2 (P_c - \eta_2^2/4)}{2(1 - \delta) \sqrt{PP_c - P\eta_2^2/4 - P_c\eta_1^2/4 + \eta_1^2\eta_2^2/16}} \left(1 + \frac{\epsilon_1 - \epsilon_2 - \delta\epsilon_3 + \delta\epsilon_4}{1 - \delta} \right),
\end{aligned} \tag{52}$$

$$\begin{aligned}
\frac{1}{n} \frac{d\xi_1}{dt} &= \frac{\eta_1 P}{(1 - \delta)^2} (\epsilon_1 - \epsilon_2 - \delta\epsilon_3 + \delta\epsilon_4) + \frac{\eta_1 P_c}{1 - \delta} + \frac{\eta_1^3}{2(1 - \delta)^2} (-\epsilon_1 + \epsilon_2 + \delta\epsilon_3 - \delta\epsilon_4) - \frac{\eta_1 \eta_2^2}{2(1 - \delta)} \\
&+ \frac{\eta_1^2 \eta_2 (\eta_2^2/4 - P_c)}{4(1 - \delta) \sqrt{PP_c - P\eta_2^2/4 - P_c\eta_1^2/4 + \eta_1^2\eta_2^2/16}} \left(1 + \frac{\epsilon_1 - \epsilon_2 - \delta\epsilon_3 + \delta\epsilon_4}{1 - \delta} \right) \\
&+ \frac{\eta_2}{1 - \delta} \sqrt{PP_c - P\eta_2^2/4 - P_c\eta_1^2/4 + \eta_1^2\eta_2^2/16} \left(1 + \frac{\epsilon_1 - \epsilon_2 - \delta\epsilon_3 + \delta\epsilon_4}{1 - \delta} \right),
\end{aligned} \tag{53}$$

and

$$\begin{aligned}
\frac{1}{n} \frac{d\xi_2}{dt} &= \frac{\eta_2 P_c}{(1 - \delta)^2} \left(\epsilon_1 - \epsilon_2 + \left(\frac{1}{\delta} - 2 \right) \epsilon_3 + \left(2 - \frac{1}{\delta} \right) \epsilon_4 \right) + \frac{\eta_2 P}{1 - \delta} \\
&+ \frac{\eta_2^3}{2(1 - \delta)^2} \left(-\epsilon_1 + \epsilon_2 + \left(2 - \frac{1}{\delta} \right) \epsilon_3 + \left(\frac{1}{\delta} - 2 \right) \epsilon_4 \right) - \frac{\eta_1^2 \eta_2}{2(1 - \delta)} \\
&+ \frac{\eta_1 \eta_2^2 (\eta_1^2/4 - P)}{4(1 - \delta) \sqrt{PP_c - P\eta_2^2/4 - P_c\eta_1^2/4 + \eta_1^2\eta_2^2/16}} \left(1 + \frac{\epsilon_1 - \epsilon_2 - \delta\epsilon_3 + \delta\epsilon_4}{1 - \delta} \right) \\
&+ \frac{\eta_1}{1 - \delta} \sqrt{PP_c - P\eta_2^2/4 - P_c\eta_1^2/4 + \eta_1^2\eta_2^2/16} \left(1 + \frac{\epsilon_1 - \epsilon_2 - \delta\epsilon_3 + \delta\epsilon_4}{1 - \delta} \right).
\end{aligned} \tag{54}$$

For $\epsilon_3 = 10\epsilon_1$, $\epsilon_4 = 0$ and $\delta = 0.5$, the real roots of this system are

- $P = 1.046772470$, $\eta_1 = 1.446908787$, $\eta_2 = -1.023119016$
- $P = 1.002812138$, $\eta_1 = 0.2502391659$, $\eta_2 = -0.1690724173$

Table 18 Location of a new stable equilibrium, determined analytically (a) thanks to Eq.52 to 54 and numerically (n), for $\delta = 0.5$. The last column, A , gives the amplitude of the 1.77-d longitudinal librations, obtained in our numerical code. Here, only the equilibrium corresponding to $\eta_1 > 0$ and $\eta_2 < 0$ has been considered. In all these cases, another stable equilibrium exists in changing the signs of η_1 and η_2 .

ϵ_3/ϵ_1	ϵ_4/ϵ_2	$P - 1$ (n)	$P - 1$ (a)	η_1 (n)	η_1 (a)	η_2 (n)	η_2 (a)
9.45	0	1.5831×10^{-4}	4.0680×10^{-4}	0.0608	0.0972	-0.0411	-0.0657
10	0	2.8103×10^{-3}	2.8121×10^{-3}	0.2502	0.2502	-0.1690	-0.1691
10	0.3	1.9482×10^{-3}	1.9501×10^{-3}	0.2099	0.2100	-0.1418	-0.1419

- $P = 1, \eta_1 = \eta_2 = 0$
- $P = 1.002812138, \eta_1 = -0.2502391659, \eta_2 = 0.1690724173$
- $P = 0.3489241565, \eta_1 = 0.8353731582, \eta_2 = -0.5606980247$

while they are, for $\epsilon_3 = 9\epsilon_1, \epsilon_4 = 0$ and $\delta = 0.5$:

- $P = 1.041484268, \eta_1 = -1.443249317, \eta_2 = -1.020531379$
- $P = 0.3471614224, \eta_1 = -0.8332603709, \eta_2 = -0.5892040580$
- $P = 1, \eta_1 = \eta_2 = 0$
- $P = 0.9978852209, \eta_1 = -2.010693353, \eta_2 = -1.421011855.$

So, we can see for $P \approx 1$ and $|\eta_1|, |\eta_2| < 0.5$, an appearance of 2 additional equilibria. In order to test the validity of this analytical study, we propose (Tab.18) a short comparison between its results and the numerical results, in 3 cases where the 2 equilibria appear. We can see a significant discrepancy for the first case, where $\epsilon_3 = 9.45\epsilon_1$ and $\epsilon_4 = 0$. In this case, the equilibria are close to the origin $\eta_1 = \eta_2 = 0$, while a good agreement is reached for the other two cases, where the equilibrium values of η_1 and η_2 are bigger. The observed discrepancy can be due to the neglect of the obliquity, the inclination and the eccentricity.

We now propose to study the existence of these 2 additional equilibria. Since their existence is linked to the stability of the equilibrium corresponding to $\eta_i, \xi_i = 0, P = 1$ and $P_c = \delta$, we in fact study this stability. In setting $\xi_1 = \xi_2 = 0, P = 1$ and $P_c = \delta$ in the averaged Hamiltonian, we get the quantity \mathcal{S} :

$$\begin{aligned}
\mathcal{S}(\eta_1, \eta_2) &= \alpha - 1 + \frac{1 - \delta + \eta_1^2 \delta + \eta_2^2 - \eta_1^2 \eta_2^2 / 2}{2(1 - \delta)} \\
&+ \epsilon_1 \left(-\frac{3}{2} + \frac{\eta_1^2 + \eta_2^2 \delta - (\eta_1^4 + \eta_2^4) / 4}{2(1 - \delta)^2} + \frac{\alpha}{1 - \delta} \right) \\
&+ \epsilon_2 \left(-\frac{3}{2} - \frac{\eta_1^2 + \eta_2^2 \delta - (\eta_1^4 + \eta_2^4) / 4}{2(1 - \delta)^2} - \frac{\alpha}{1 - \delta} \right) \\
&+ (\epsilon_3 - \epsilon_4) \left(\frac{-\delta \eta_1^2 + \eta_2^2 (1 - 2\delta) + \delta \eta_1^4 / 4 + \eta_2^4 / 2 (1 - 1/(2\delta))}{2(1 - \delta)^2} - \frac{\delta \alpha}{1 - \delta} \right)
\end{aligned} \tag{55}$$

with

$$\alpha = \frac{\eta_1 \eta_2}{1 - \delta} \sqrt{\delta - \frac{\eta_1^2 \delta + \eta_2^2}{4} + \frac{\eta_1^2 \eta_2^2}{16}}. \tag{56}$$

We do not call \mathcal{S} “Hamiltonian” since two variables, i.e. ξ_1 and ξ_2 , are sets to constants, while their associated momenta η_1 and η_2 vary. The study is now equivalent to the investigation of the extrema of the surface defined by the Eq.55. In fact we study the point defined by $\eta_1 = \eta_2 = 0$, we know thanks to previous calculations that it gives null first-order derivatives of \mathcal{S} . The topological nature of this point can be investigated in studying the second order partial derivatives of \mathcal{S} . We consider the Hessian matrix

$$\begin{aligned} \mathcal{M} &= \begin{pmatrix} \frac{\partial^2 \mathcal{S}}{\partial \eta_1^2} & \frac{\partial^2 \mathcal{S}}{\partial \eta_1 \partial \eta_2} \\ \frac{\partial^2 \mathcal{S}}{\partial \eta_2 \partial \eta_1} & \frac{\partial^2 \mathcal{S}}{\partial \eta_2^2} \end{pmatrix} \\ &= \frac{1}{(\delta - 1)^2} \begin{pmatrix} \epsilon_1 - \epsilon_2 + \delta(\epsilon_4 - \epsilon_3 + 1 - \delta) & \sqrt{\delta}(1 - \delta + \epsilon_1 - \epsilon_2 + \delta(\epsilon_4 - \epsilon_3)) \\ \sqrt{\delta}(1 - \delta + \epsilon_1 - \epsilon_2 + \delta(\epsilon_4 - \epsilon_3)) & 1 - \delta + \delta(\epsilon_1 - \epsilon_2 - 2\epsilon_3 + 2\epsilon_4) \end{pmatrix}. \end{aligned} \quad (57)$$

A minimum (corresponding to a stable equilibrium) is reached when the two eigenvalues of the Hessian, $\lambda_{1,2}$, are positive. We have:

$$\lambda_1 = \beta + \frac{\sqrt{\Delta}}{2} \quad (58)$$

$$\lambda_2 = \beta - \frac{\sqrt{\Delta}}{2} \quad (59)$$

with

$$\beta = \frac{1 - \delta^2 + (\epsilon_1 - \epsilon_2)(1 + \delta) + (\epsilon_3 - \epsilon_4)(1 - 3\delta)}{2} \quad (60)$$

and

$$\begin{aligned} \Delta &= (1 - \delta^2)^2 - 2(\epsilon_1 - \epsilon_2)(1 - 7\delta + 7\delta^2 - \delta^3) + 2(\epsilon_3 - \epsilon_4)(1 - 3\delta - \delta^2 + 3\delta^3) \\ &\quad + (\epsilon_1 - \epsilon_2)^2(1 + \delta)^2 + 2(\epsilon_1\epsilon_4 + \epsilon_2\epsilon_3 - \epsilon_1\epsilon_3 - \epsilon_2\epsilon_4)(1 - 2\delta + 5\delta^2) \\ &\quad + (\epsilon_3 - \epsilon_4)^2(1 - 2\delta + \delta^2 + 4\delta^3). \end{aligned} \quad (61)$$

Numerical evaluations show that λ_1 is always positive, and that λ_2 is usually positive, except for the interior parameters given in Tab.18. In these peculiar cases, we have $\lambda_1\lambda_2 < 0$, so the considered point ($\eta_1 = \eta_2 = 0$) is a saddle point.

This study shows that the equilibrium corresponding to $J = J_c = 0$ is unstable for $\lambda_2 = 0$. This condition is independent of the mean motion and is applicable to any body in 1:1 spin-orbit resonance, in which the interior model of a rigid mantle, a fluid core and a small solid inner core composed of dense material is realistic. We have also neglected the effect of the orbital inclination and of the regression of the ascending node. This approximation is relevant, since most of the natural satellites of the giant planets have inclinations of the order of a few arcmin, and the nodal regression of Io is one of the most rapid in the Solar System. Since here this approximation gives good results, it should be available for most of the Solar System bodies in a comparable dynamical situation.

Table 19 The first case is the reference one, and the other ones correspond to the cases where two additional stable equilibria appear.

ϵ_3/ϵ_1	ϵ_4/ϵ_2	$\langle K_m \rangle$	$\langle J_m \rangle$	$\langle J_c \rangle$
1	1	2.299 am	0.155 as	21.470 as
9.45	0	9.065 am	3.632°	3.335°
10	0	37.542 am	14.975°	13.726°
10	0.3	31.220 am	12.555°	11.516°

5.3 Effect on the observable variables

We now consider the influence of this peculiar behavior on the observable parameters, i.e. data that could be observed if our pseudo-Io were real and if it were observed with enough accuracy. In particular, they have to refer to the mantle since its rotation is actually the rotation of the surface. These observable data can be deduced from the canonical variables, that give a complete mathematical description of the system.

A complete derivation of the observable outputs can be found in (Noyelles et al. [35]), we here choose to represent the following quantities:

- the mean obliquity of the mantle $\langle K_m \rangle$,
- the mean amplitude of the polar motion of the mantle $\langle J_m \rangle$,
- the mean amplitude of the polar motion of the core $\langle J_c \rangle$.

All these results are obtained thanks to frequency analysis, and they are gathered in Tab.19. We can see that the stable equilibria that appear induce a forcing of the polar motion of the surface (or mantle) of our pseudo Io (Fig.4), that can reach 15°. In (Noyelles 2008 [32]) we found a forcing of the polar motion of a rigid Titan, due to a resonance between the free wobble and the forced precession of Titan’s perihelion. We considered it as a possible explanation for the super-synchronous rotation of Titan, before it was observed (Stiles et al. 2008 & 2010 [45]). This is different here, since no resonance appears.

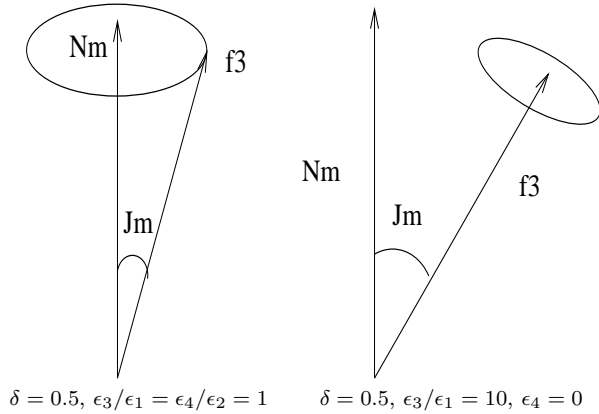


Fig. 4 Location of the North Pole of the mantle of the body (located by \mathbf{f}_3) with respect to its angular momentum \mathbf{N}_m in the classical case (left) and with a highly flattened core (right).

Table 20 The variable $K \exp(ir)$ for $\delta = 0.5$, $\epsilon_3 = 0$ and $\epsilon_2 = \epsilon_4$. The series are in complex exponential and the amplitudes in arcseconds. We can note a nearly constant component ν , that has a negligible in the usual case.

	Amplitude (arcsec)	Frequency (rad/y)	Phase (t=0)	T (d)	Identification
1	84.516	1.093×10^{-4}	78.801°	2.1×10^7	ν
2	66.484	0.8455888	-5.730°	2714.006	$-\delta\Omega_o$
3	0.022	-2595.2545339	5.730°	0.884	$\delta\Omega_o - 2\lambda_o$
4	0.006	1296.2314632	-35.742°	1.770	$\lambda_o - \varpi_o + \nu$
5	0.006	-1296.2312447	-166.558°	1.770	$\varpi_o - \lambda_o + \nu$
6	0.005	-1295.3857651	-71.138°	1.772	$\varpi_o - \lambda_o - \delta\Omega_o - \pi$
7	0.005	1297.0769428	59.679°	1.769	$\lambda_o - \varpi_o - \delta\Omega_o + \pi$

6 Orientation of the angular momentum

Among the Third Cassini Law (see e.g. Cassini (1693) [4] or Colombo (1966) [6]), the equilibrium orientation of the total angular momentum of the body is assumed to be in the Cassini State 1. As a consequence, the angular momentum, the normal to the orbital plane and the normal to the Laplace Plane are coplanar, the Laplace Plane being a reference plane based on the precessional motion of the orbital ascending node, that minimizes the variations of the inclination of the considered body. There are in fact several ways to define this plane, as for instance in (Yseboodt et al. 2006 [51]) or in (D’Hoedt et al. [10]). A difficulty is: how to consider a constant reference plane if the precession rate of the ascending node is not constant? Should we average over a “long enough” time interval, or over a time-interval suitable to the observations of a space mission?

The reader can find in (Noyelles 2009 [33]) a discussion on the choice of an “appropriate” reference plane depending on the variations of the orbital inclination, that allows the argument $\rho = \Omega_o - h$ to librate. It is shown that, for the rotation of a rigid body in 1:1 spin-orbit resonance, if the satellite orbits close to its parent planet, the precessional motion is ruled by the oblateness of the planet (its J_2) and so its precession rate is close to be constant. In such a case, choosing the equatorial plane of the planet as a reference plane to describe the behavior of the angular momentum of the body can be a convenient choice. However, when the satellite orbits far from its parent planet as it is the case for Titan or Callisto, the reference plane for the nodal precession is shifted because of the Solar gravitational perturbation. In such a case, considering the planet’s equatorial plane as the reference plane could either result in a oscillating rotation node h as it is the case for Titan (Noyelles et al. 2008 [31]), either result in an erratic apparent behavior due to an improper choice of the reference plane, as is the case for Callisto (Noyelles 2009 [33]).

In our case of a pseudo-Io with a constant regression of the node, no “strange” behavior is expected. In particular, the Tab.6 supports the assumption of a quasi-periodic behavior of the difference of the nodes ρ . However, we have found a different behavior for a small flattening of the core ϵ_3 (Fig.5 and Tab.20) resulting in a significant shift of the mean equilibrium orientation of the total angular momentum. This shift seems to be not constant but a long-period oscillation, the period being $\approx 57,000$ years. We call ν this oscillation.

In (Noyelles et al. 2010 [35]), we had found a particular behavior for small ϵ_3 , that we attributed to the exact resonance between the Free Core Nutation frequency ω_z

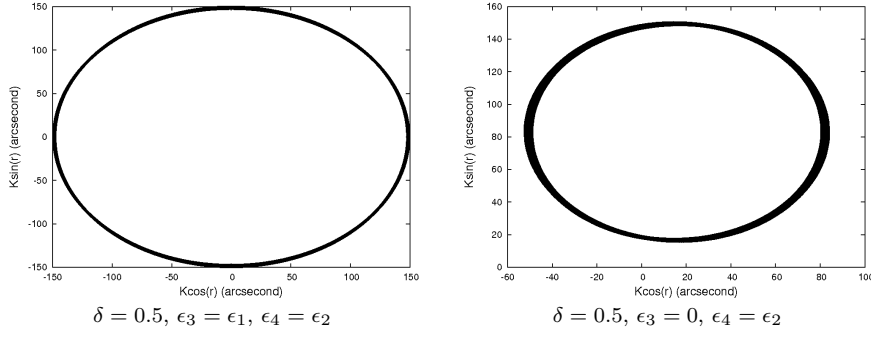


Fig. 5 Behavior of the orientation of the angular momentum of our pseudo Io $K \exp i r$, with 2 different internal structure models, in the inertial reference frame. The right panel shows a shift of this motion that is not on averaged at the origin.

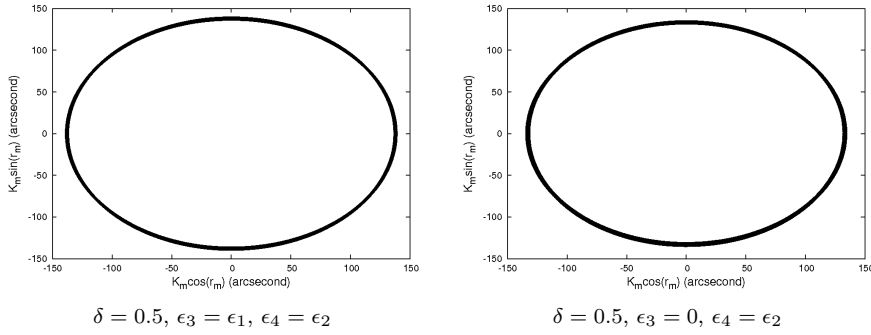


Fig. 6 Behavior of the orientation of the angular momentum of the mantle (i.e. the surface) of our pseudo Io $K_m \exp i r_m$, with 2 different internal structure models, in the inertial reference frame. Contrary to the total angular momentum (Fig.5), it does not exhibit particular behavior.

and the spin frequency. We also noticed an asymptotic behavior of the free frequency ω_v that tended to 0 (and the period T_v to infinity) when ϵ_3 tended to 0. This last behavior is here observed as well as can be seen in Tab.10. This is confirmed by some tests at $\epsilon_3 = \epsilon_1/10$ suggesting $T_v = 9933.75$ days. However, even if the free period T_z gets closer to the spin period of 1.76799 day, it does not seem to reach it. So we cannot speak of resonant behavior, it seems more likely to be a kind of singularity at $\epsilon_3 = 0$.

The Fig.6 shows the orientation of the angular momentum of the mantle/surface, that does not exhibit this shift. So, if such a situation would occur (i.e. very small polar flattening of the core), the equatorial/ring plane of the planet could be an acceptable reference plane to describe the orientation of this axis. In fact, a physical signature of this dynamics remains in the core, we indeed get a mean J_c of ≈ 3 arcmin for $\epsilon_3 = 0$ while we have $\langle J_c \rangle \approx 21$ arcsec for $\epsilon_3 = \epsilon_1$.

7 Conclusion

In this study we have presented the behavior of a pseudo-Io orbit on a low eccentric orbit around its parent planet, with a uniform nodal regression and a constant inclination,

in considering it as a two-layer body composed of a rigid mantle and a fluid triaxial core. This model can be applied to study the rotation of most differentiated natural satellites.

We have described the “usual” case, consisting of small oscillations around the expected equilibrium, i.e. synchronous rotation with a small obliquity and no polar motion, but we also have, especially for a highly flattened core, another behavior resulting in a polar motion forced by several degrees. Another peculiar behavior is when the polar flattening of the core is very small. In this last case we have a forcing of the obliquity of the full body, but not of its mantle, so there should be no observational evidence of this phenomenon. From a mathematical point of view, this could be due to a kind of singularity in the parameter ϵ_3 .

This study aimed at exploring the behavior of a model, its application to real bodies would require to consider complete ephemerides. This would add additional forcing frequencies complicating the dynamics of the system. New behavior cannot a priori be excluded.

A possibility to improve the model would be to consider nonlinear phenomena in the fluid, but this is another story...

Acknowledgements Numerical simulations were made on the local computing resources (*Cluster URBM-SYSDYN*) at the University of Namur (FUNDP, Belgium). The author is indebted to Nicolas Delsate and Julien Frouard for fruitful discussions. BN is F.R.S.-FNRS post-doctoral research fellow.

A The NAFF algorithm

The frequency analysis algorithm that we use is based on Laskar’s original idea, named NAFF as Numerical Analysis of the Fundamental Frequencies (see for instance Laskar 1993 [26] for the method, and Laskar 2005 [27] for the convergence proofs). It aims at identifying the coefficients a_k and ω_k of a complex signal $f(t)$ obtained numerically over a finite time span $[-T; T]$ and verifying

$$f(t) \approx \sum_{k=1}^n a_k \exp(i\omega_k t), \quad (62)$$

where ω_k are real frequencies and a_k complex coefficients. If the signal $f(t)$ is real, its frequency spectrum is symmetric and the complex amplitudes associated with the frequencies ω_k and $-\omega_k$ are complex conjugates. The frequencies and amplitudes associated are found with an iterative scheme. To determine the first frequency ω_1 , one searches for the maximum of the amplitude of

$$\phi(\omega) = \langle f(t), \exp(i\omega t) \rangle, \quad (63)$$

where the scalar product $\langle f(t), g(t) \rangle$ is defined by

$$\langle f(t), g(t) \rangle = \frac{1}{2T} \int_{-T}^T f(t)g(t)^* \chi(t) dt, \quad (64)$$

$g(t)^*$ being the complex conjugate of $g(t)$. $\chi(t)$ is a weight function alike a Hann or a Hamming window, i.e. a positive function verifying

$$\frac{1}{2T} \int_{-T}^T \chi(t) dt = 1. \quad (65)$$

Using such a window can help the determination in reducing the amplitude of secondary minima in the transform (64). Its use is optional.

Once the first periodic term $\exp(i\omega_1 t)$ is found, its complex amplitude a_1 is obtained by orthogonal projection, and the process is started again on the remainder $f_1(t) = f(t) - a_1 \exp(i\omega_1 t)$. The algorithm stops when two detected frequencies are too close to each other, what alters their determinations, or when the number of detected terms reaches a limit set by the user. This algorithm is very efficient, except when two frequencies are too close to each other. In that case, the algorithm is not confident in its accuracy and stops. When the difference between two frequencies is larger than twice the frequency associated with the length of the total time interval, the determination of each fundamental frequency is not perturbed by the other ones. Although the iterative method suggested by Champenois [5] allows to reduce this distance, some troubles may remain. In our particular case, these problems are likely to arise because of the proximity between the free frequency of the core ω_z and the frequency of the spin.

References

1. Anderson, J.D., Jacobson, R.A., Lau, E.L. et al.: Io's gravity field and interior structure, *Journal of Geophysical Research*, **106**, 32963-32969 (2001)
2. Andoyer, H.: *Mécanique Céleste*, Gauthier-Villars, Paris (1926)
3. Bouquillon, S., Kinoshita, H., Souchay J.: Extension of Cassini's laws, *Celestial Mechanics and Dynamical Astronomy*, **86**, 29-57 (2003)
4. Cassini, G.D.: *Traité de l'origine et du progrès de l'astronomie*, Paris (1693)
5. Champenois, S.: *Dynamique de la résonance entre Mimas et Téthys, premier et troisième satellites de Saturne*, Ph.D. Thesis, Observatoire de Paris (1998)
6. Colombo, G.: Cassini's Second and Third Laws, *The Astronomical Journal*, **71**, 891-896 (1966)
7. Comstock, R.L., Bills, B.G.: A solar system survey of forced librations in longitude, *Journal of Geophysical Research*, **108**(E09), 5100 (2003)
8. Couetdic, J., Laskar, J., Correia, A.C.M., Mayor, M., Udry, S.: Dynamical stability analysis of the HD202206 system and constraints to the planetary orbits, *Astronomy and Astrophysics*, **519**, A10 (2010)
9. Delsate, N.: Analytical and numerical study of the ground-track resonances of Dawn orbiting Vesta, *Planetary and Space Science*, **59**, 1372-1383 (2011)
10. D'Hoedt, S., Noyelles, B., Dufey, J., Lemaître, A.: Determination of an instantaneous Laplace plane for Mercury's rotation, *Advances in Space Research*, **44**, 597-603 (2009)
11. Dufey, J., Noyelles, B., Rambaux, N., Lemaître, A.: Latitudinal librations of Mercury with a fluid core, *Icarus*, **203**, 1-12 (2009)
12. Edgeworth, R., Dalton, B.J., Parnell, T.: The pitch drop experiment, *European Journal of Physics*, **5**, 198-200 (1984)
13. Getino, J.: Forced nutations of a rigid mantle - liquid core Earth model in canonical formulation, *Geophysical Journal International*, **122**, 803-814 (1995)
14. Getino, J., Ferrándiz, J.M.: On the effect of the mantle elasticity on the Earth's rotation, *Celestial Mechanics and Dynamical Astronomy*, **61**, 117-180 (1995)
15. Getino, J., Ferrándiz, J.M.: A Hamiltonian approach to dissipative phenomena between Earth mantle and core, and effects on free nutations, *Geophysical Journal International*, **130**, 326-334 (1997)
16. Goldreich, P., Peale, S.J.: Spin-orbit coupling in the solar system, *The Astronomical Journal*, **71**, 425-438 (1966)
17. Greenspan, H.P.: *The theory of rotating fluids*, Cambridge University Press, Cambridge (1968)
18. Henrard, J.: Virtual singularities in the artificial satellite theory, *Celestial Mechanics*, **10**, 437-449 (1974)
19. Henrard, J.: The rotation of Io, *Icarus*, **178**, 144-153 (2005)
20. Henrard, J.: The rotation of Europa, *Celestial Mechanics and Dynamical Astronomy*, **91**, 131-149 (2005)
21. Henrard, J.: The rotation of Io with a fluid core, *Celestial Mechanics and Dynamical Astronomy*, **101**, 1-12 (2008)
22. Hough, S.S.: The oscillations of a rotating ellipsoidal shell containing fluid, *Philos. Trans. R. Soc. London A*, **186**, 469-506 (1895)

23. Kerswell, R.R., Malkus, W.V.R.: Tidal instability as the source for Io's magnetic signature, *Geophysical Research Letters*, **25**, 603-606 (1998)
24. Koziel, K.: The constants of the Moon's physical libration derived on the basis of four series of heliometric observations from the years 1877 to 1915, *Icarus*, **7**, 1-28 (1967)
25. Lainey, V., Duriez, L., Vienne, A.: Synthetic representation of the Galilean satellites' orbital motions from L1 ephemerides, *Astronomy & Astrophysics*, **456**, 783-788 (2006)
26. Laskar, J.: Frequency analysis of a dynamical system, *Celestial Mechanics and Dynamical Astronomy*, **56**, 191-196 (1993)
27. Laskar, J.: Frequency map analysis and quasiperiodic decomposition, in *Hamiltonian systems and Fourier analysis: new prospects for gravitational dynamics*, Benest et al. editors, Cambridge Sci. Publ., 99-129 (2005)
28. Lorenz, R.D., Stiles, B.W., Kirk, R.L. et al.: Titan's rotation reveals an internal ocean and changing zonal winds, *Science*, **319**, 1649-1651 (2008)
29. Margot, J.-L., Peale, S.J., Jurgens, R.F. et al.: Large longitude libration of Mercury reveals a molten core, *Science*, **316**, 710-714 (2007)
30. Meyer, J., Wisdom, J.: Note: Precession of the lunar core, *Icarus*, **211**, 921-924 (2011)
31. Noyelles, B., Lemaître, A., Vienne, A.: Titan's rotation: A 3-dimensional theory, *Astronomy and Astrophysics*, **478**, 959-970 (2008)
32. Noyelles, B.: Titan's rotational state: The effects of a forced "free" resonant wobble, *Celestial Mechanics and Dynamical Astronomy*, **101**, 13-30 (2008)
33. Noyelles, B.: Expression of Cassini's third law for Callisto, and theory of its rotation, *Icarus*, **202**, 225-239 (2009)
34. Noyelles, B.: Theory of the rotation of Janus and Epimetheus, *Icarus*, **207**, 887-902 (2010)
35. Noyelles, B., Dufey, J., Lemaître, A.: Core-mantle interactions for Mercury, *MNRAS*, **407**, 479-496 (2010)
36. Noyelles, B., Delsate, N., Carletti, T.: Equilibrium search algorithm of a perturbed quasi-integrable system: NAFFO, arXiv:1101.2138, submitted (2011)
37. Peale, S.J.: Generalized Cassini's laws, *The Astronomical Journal*, **74**, 483-489 (1969)
38. Poincaré, H.: Sur la précession des corps déformables, *Bulletin Astronomique*, **27**, 321-357 (1910)
39. Porco, C.C., Helfenstein, P., Thomas, P.C. et al.: Cassini observes the active South Pole of Enceladus, *Science*, **311**, 1393-1400 (2006)
40. Rambaux, N., Van Hoolst, T., Dehant, V., Bois, E.: Inertial core-mantle coupling and libration of Mercury, *Astronomy and Astrophysics*, **468**, 711-719 (2007)
41. Rambaux, N., Van Hoolst, T., Karatekin, Ö.: Librational response of Europa, Ganymede, and Callisto with an ocean for a non-Keplerian orbit, *Astronomy and Astrophysics*, **527**, A118 (2011)
42. Rambaux, N., Williams, J.G.: The Moon's physical librations and determination of their free modes, *Celestial Mechanics and Dynamical Astronomy*, **109**, 85-100 (2011)
43. Robutel, P., Rambaux, N., Castillo-Rogez, J.: Analytical description of physical librations of saturnian coorbital satellites Janus and Epimetheus, *Icarus*, **211**, 758-769 (2011)
44. Rutter, M.D., Secco, R.A., Uchida, T., Hongjian, L., Wang, Y., Rivers, M.L., Sutton, S.R.: Towards evaluating the viscosity of the Earth's outer core: An experimental high pressure study of liquid Fe-S (8.5 wt.% S), *Geophysical Research Letters*, **29**, 1217 (2002)
45. Stiles, B.W., Kirk, R.L., Lorenz, R.D., Hensley, S., Lee, E., Ostro, S.J., Allison, M.D., Callahan, P.S., Gim, Y., Iess, L., Persi Del Marmo, P., Hamilton, G., Johnson, W.T.K., West, R.D.: Determining Titan's spin state from CASSINI RADAR images, *The Astronomical Journal*, **135**, 1669-1680 (2008), Erratum: *The Astronomical Journal*, **139**, 311 (2010)
46. Tiscareno, M.S., Thomas, P.C., Burns, J.A.: The rotation of Janus and Epimetheus, *Icarus*, **204**, 254-261 (2009)
47. Tokano, T., Van Hoolst, T., Karatekin, Ö.: Polar motion of Titan forced by the atmosphere, *Journal of Geophysical Research*, **116**, E05002 (2011)
48. Touma, J., Wisdom, J.: Nonlinear core-mantle coupling, *The Astronomical Journal*, **122**, 1030-1050 (2001)
49. Ward, W.R., Hamilton, D.P.: Tilting Saturn. I. Analytical model, *The Astronomical Journal*, **128**, 2501-2509 (2004)
50. Williams, J.G., Slade, M.A., Eckhardt, D.H., Kaula, W.M.: Lunar physical librations and laser ranging, *Moon*, **8**, 469-483 (1973)
51. Yseboodt, M., Margot, J.-L.: Evolution of Mercury's obliquity, *Icarus*, **181**, 327-337 (2006)